Natural Resources Canada | Ressources naturelles Canada

GEOLOGICAL SURVEY OF CANADA
OPEN FILE 8617

Conversion of seismic-reflection time to depth for the Labrador margin, Davis Strait, and Baffin Bay, offshore northern Canada and Greenland, using sonic logs, checkshot surveys, and wide-angle seismic velocities

C.E. Keen

2019

Canada

GEOLOGICAL SURVEY OF CANADA
OPEN FILE 8617

Conversion of seismic-reflection time to depth for the Labrador margin, Davis Strait, and Baffin Bay, offshore northern Canada and Greenland, using sonic logs, checkshot surveys, and wide-angle seismic velocities

C.E. Keen

Geological Survey of Canada, 1 Challenger Drive, P.O. Box 1006, Dartmouth, Nova Scotia B2Y 4A2

2019

Permanent link: https://doi.org/10.4095/315016

This publication is available for free download through GEOSCAN (https://geoscan.nrcan.gc.ca/).

Recommended citation

Keen, C.E., 2019. Conversion of seismic-reflection time to depth for the Labrador margin, Davis Strait, and Baffin Bay, offshore northern Canada and Greenland, using sonic logs, checkshot surveys, and wide-angle seismic velocities; Geological Survey of Canada, Open File 8617, 42 p. https://doi.org/10.4095/315016

Publications in this series have not been edited; they are released as submitted by the author

Conversion of seismic-reflection time to depth for the Labrador margin, Davis Strait, and Baffin Bay, offshore northern Canada and Greenland, using sonic logs, checkshot surveys, and wide-angle seismic velocities

C.E. Keen

TABLE OF CONTENTS

LIST OF TABLES

LIST OF FIGURES

1. INTRODUCTION

The purpose of this study is to determine regional time-depth relationships within the sediments on the Labrador continental margin, in the Davis Strait region, and in Baffin Bay (Fig. 1). Various datasets have been used, depending on their distribution and accuracy. The datasets include sonic logs from deep exploratory wells, checkshot surveys at selected wells, and wide-angle seismic reflection and refraction measurements. The resulting velocity- and time-depth relationships can be used to convert seismic reflection times to depth. Velocity-depth distributions, extracted from these datasets, can also be used to obtain porosity-depth relationships and the latter used to estimate densities and compaction of sediments. In the Labrador Sea region previous related studies include those of Royden and Keen (1980), Issler (1987), Issler and Beaumont (1987) and Li et al., (2014). Data on lithology and stratigraphy, as well as acoustic log data, were obtained using the BASIN database of GSC Atlantic (http://basin.gdr.nrcan.gc.ca) and from GEUS (Geological Survey of Denmark and Greenland). Lithologies in these regions fall primarily on the sandstone-shale continuum, with minor amounts of limestone (Balkwill and McMillan, 1990). In addition, recent velocity-depth measurements from wide-angle seismic studies were used to augment the well data, particularly in Davis Strait and Baffin Bay (Chian et al, 1995; Altenberndt et al., 2014; 2015; 2016; Funck et al., 2007; 2012; Sukro et al., 2012; 2013). In the latter region we have virtually no available well data. The single ODP 645 well did not record reliable log data and only sampled the shallower part of the sedimentary section (Srivastava et al., 1987). We will consider the three regions separately: Labrador margin , Davis Strait and Baffin Bay, since the nature of data in each differs (Fig. 1). We do not sub-divide these regions further, as the data at present is not sufficient to do this in a consistent manner. Data for the Mesozoic-Cenozoic sediments which form the syn-rift and post-rift sediment packages in these regions are analyzed, and we do not include older, pre-rift sediments.

2. LABRADOR

We start with the Labrador shelf where there are 23 exploratory wells which were used in the analysis. These data allow the investigation of the two major controlling factors in the velocity-depth relationship:1) depth of burial within the sedimentary section which leads to compaction, and 2) variations due to changes in lithology. Table 1 shows the data available at each of these wells.

2.1 Sonic Logs

Transit time (dt=1/velocity) is obtained directly from the sonic logs as a function of depth. The log values were averaged over 60 m depth intervals, except for the relatively thin Leif and Gudrid sand units which were averaged over 30m . Results are shown in Figures 2 to 6.

We use a least squares fit to the data , dt-dt_{ma}, where dt_{ma} is the matrix slowness, $1/v_{ma}$, and v_{ma} is the matrix velocity, the highest velocity approached at great depth where porosity tends to zero. We choose a values of dt_{ma} typically used in well log analysis (Issler, 1992; Raiga-Clemenceau et al., 1988). A matrix slowness of 222 µsec/m (4.5 km/s) was used for shale, mudstone and a value of 182 µsec/m (5.5km/s) was used for sandstone. We fit exponential functions to the sonic log data using least squares anlysis:

$$dt-dt_{ma}=k\exp(-lz).$$

This fitted curve can be integrated analytically to give a depth-time curve:

$$t=dt_{ma}z+k\ (1.-\exp(-lz))/l$$

where parameters k and l are found from the least squares fit to the data; dt_{ma} is given above, and t and z are the time and depth, respectively. Time and depth are always measured with respect to the sea floor unless otherwise stated. Since the above function is difficult to evaluate for z, we fit the t,z values with a second order polynomial using least squares, which gives a simple function for z: $z=a+bt+ct^2$ as well as a good fit to the t,z pairs. The use of the polynomial function does not introduce significant error into the results and higher order polynomials do not give a significantly better fit. The constants (k,l) are listed in Table 3 and the polynomial constants (a,b,c) for the final selection of time-depth functions are given in Table 4.

The sonic log data for all wells were first merged into 2 groups, corresponding to shales/mudstones and sandstones. On a regional basis, the Saglek and Bjarni Formations, and the Gudrid, Leif and Freydis members are sandstones and formed one group, while the Mokami, Kenamu, Cartwright and Markland Formations are finer grained and formed the second group (see Balkwill and McMillan, 1990 for detailed description of these Formations). We ignore here minor amounts of limestone and other constituents, as they are insignificant on a regional scale. As discussed below, after a general analysis based on the above two groups, we take a closer look at lithology using the CanStrat data in the BASIN database. The CanStrat data details the percentage of sand versus shale for these wells and we use this data to determine the variability in lithology within these formations. This is important because sandy Formations can be locally fine-grained and vice versa, and therefore is not always a reliable measure of lithology. Table 2 shows the lithologies for each depth interval in each well used in the analysis obtained from the CanStrat database. It can be seen that the shale content of the fine-grained units defined on the basis of Formation is generally higher than 80% , supporting the merging of sonic logs in this case. The sandy units are more variable.

Figure 2 shows all the sonic log data, separated into the 2 groups of 'sands' and 'finer-grained' lithologies on the basis of their corresponding Formation. Given the scatter of the data points, there is little detectable difference in the transit time distributions for sands and fine-grained units, with the exception of the Bjarni Formation which lies below about 2000m and exhibits higher average velocities (lower transit times) than the other units. Except for this formation it appears that compaction, not lithology, plays a dominant role in the velocity increase with depth. The scatter of these data cannot be attributed to depth of burial or gross lithological changes and introduce significant uncertainty into the data fitting process. In particular there are some very low transit times, approaching the matrix transit time for sandstone, between about 1500 and 2500 m, which are outliers and difficult to explain with the current data. These outliers are not limited to a particular lithology or formation.

Looking further at the issue of lithology, the % shales within finer-grained units (Table 2) does not seem to affect the transit times in a systematic manner (Fig. 3), probably because all these units exhibit a fairly high proportion of shales. However, the ‘sandstones’ group are more variable in lithology; there is a wide variability in the % sand, down to a low of 10% (see Table 2). Figure 4 shows a comparison of all ‘sandstone’ results, highlighting those that exhibit a higher sand content (greater than 70%). There is no clear division of these data into particular groupings, except that the Bjarni Formation consistently exhibits lower transit times (higher velocities) below about 2000 m when the sand content is high. We can only determine from the present data that the high sand content intervals, generally corresponding to the Bjarni Formation, exhibits a significantly different velocity-depth relationship compared to other intervals. A time-depth polynomial function for the 'very sandy' Bjarni Formation is given in Table 4.

Given the above observations we would be justified in dividing the sediments into two layers on the basis of velocity: a 'sandy' Bjarni lower layer and all overlying formations. However, the high sand content layer has been sampled only in a vicinity of the Bjarni wells (Bjarni O-82 , Bjarni H-81, Herjolf M-92, North Bjarni F-08) and in proximal grabens (Tyrk P-100 and Freydis B-87). It is not clear how this sandy lower layer is distributed over large parts of the Labrador shelf and slope, and whether it occurs in the more distal regions of the Labrador margin. Therefore, on a broad regional basis it is not clear that the presence of a high velocity lower sedimentary layer is a realistic assumption. For this reason, we have grouped all the sediments into one unit, and derived the average time-depth curve for all lithologies. This result is also listed in Table 4.

The simplifying assumption of a single lithological unit is supported by the low seismic velocities at great depth within the sediments reported in wide-angle seismic studies. On profile 90-1 in the Hopedale Basin (Fig. 1; Chian et al., 1995) the highest sediment velocity is about 4.0 km/s at a depth of burial of 9 km. At this great depth, a limiting maximum velocity would be expected, as porosity tends toward 0. This measured seismic velocity is much lower than the matrix velocity for sandstone (5.5km/s; dtma=182 µsec/m) and closer to that for shales (4.5 km/s; 222 µsec/m), supporting the absence of a significant high-velocity sandstone layer at the base of the sedimentary column below the outer shelf in the Hopedale Basin area. Similar results (4.3 km/s at 8 km depth) are obtained in the Saglek Basin (line 5e, Fig. 1, Funck and Louden, 1999).

2.2 Porosity-Depth relationship

Finally, it is useful to note that the expression for dt versus depth used here; $dt\text{-}dt_{ma}=k\exp(-lz)$, is related to a common porosity-depth relationship (e.g. Royden and Keen, 1980), which is also expressed as an exponential function: $\phi=\phi_o\exp(-lz)$, where ϕ_o=porosity at the sea floor. Since the porosity is related to the transit time; $dt=\phi dt_w+(1.-\phi)dt_{ma}$, $\phi_o=k/(dt_w-dt_{ma})$. dt_w=transit time in water. The porosity relationship is useful in studies where the compaction of sediments is required and can be derived from the parameters l and k provided in Table 3.

2.3 Checkshot Surveys

Checkshot surveys, where available, were used independently to find the velocity-depth distribution. There were 15 wells used for this analysis on the Labrador margin (Table 1). The slope of the time-depth plots from the checkshot surveys can be compared with the sonic logs, and it can be seen that both datasets fall within the same data space (Figs. 5 and 6). The high velocities in the Bjarni Formation are seen in both datasets (Fig. 6). However, the checkshot data points are more widely spaced in depth and therefore the travel times are typically averaged over depths of about 100 to 300 m and often cross lithological boundaries. The sonic log results from the 30-60m averages show more scatter than the checkshots. They are probably more precise in terms of measuring velocity over a short depth range. Sonic logs do not provide data in the uppermost sediments. In contrast, the checkshots may provide more representative averages over greater depth ranges, and include the uppermost sediments. However, since the checkshots measure cumulative travel times to a given depth and may include several lithologies along their raypaths, it is difficult to separate the effects of changing lithololgy with depth.

The derived time-depth curves are presented in Figure 7 (see Table 4 for polynomial coefficients). All lithologies are included. Although initial analysis did include separation into shales and sandstones as shown in Figs. 5 and 6, final results represent an average of all the lithological units, for reasons described in the previous section for the sonic log results, as well as the difficulties in separating the lithologies in the checkshot data case. We compare the checkshot and sonic log

results. The sonic log function for high sand content lithologies, as described in the previous section, reflects the higher velocities associated with the Bjarn Formation. The "all lithologies' sonic log curve is almost identical to the checkshot results, which supports the methods used. The time-depth curve derived for the central Labrador Sea region (Li et al., 2014) is also shown for comparison, and exhibits a somewhat lower velocity at shallow depths, as might be expected in deep-water, fine-grained sediments farther from land. The results show that either sonic logs or checkshots can be used for depth-time conversion, as the two functions are almost indistinguishable over the depth range of interest.

An important limiting factor is that the wells only sample the upper 4000-4500m of the sediment column, and for sediments at greater depths we must use wide-angle seismic velocities, where available, to constrain the time-depth curves. Estimates of wide-angle seismic velocity at greater depths are available on both the northern (Funck and Louden, 1999) and the central (Chian et al., 1995) Labrador shelf. These data, however, are sparse and yield only an average velocity in the deeper sediments. In Figure 8 the time-depth data points corresponding to these seismic measurements are compared to the checkshot and sonic log functions, extrapolated to greater depths. As mentioned above, low seismic velocities of 4.0 to 4.3 km/s are measured at depths of 8 to 9 km below the sedimentary basins on the shelf. This is slightly less than the 4.5 km/s for shale that was assumed in the analysis of the sonic logs for shales but overall the comparison of seismic data to the checkshot data is quite good, given the extrapolations involved and errors in both refraction and log data analysis. Velocities predicted for sand are much higher (Fig. 7), 5.08 km/s at 9 km depth which is not observed in the wide-angle seismic data, and there is lack of good data confirming the regional distribution of the higher velocity Bjarni Formation.

We conclude that the similarity of the sonic log results and the checkshots, and the successful extrapolation of the checkshot time-depth function to greater depths when compared to seismic refraction measurements, supports the use of the checkshot survey data to derive the depth-time curve. Sonic logs would give very similar results. No division into lithological units is warranted at present.

2.4 Predictions of depths versus measured depths in wells

Finally we checked the fitted checkshot function against observed depths at the wells. Where possible we compared these well depths with those predicted from the time-depth function, given the observed seismic reflection time to basement. Where basement was not observed, or was a questionable pick on the seismic data, a deep horizon within the sediment column was used instead. We found that the rms average difference between the predicted and measured depths for 21 wells is 128 m.

3. DAVIS STRAIT

In Davis Strait seismic reflection profiles show large vertical variations in basement, with local uplift and erosion likely creating velocity discontinuities and exhibiting higher velocities at shallower depths in the sediments (e.g. Funck et al.,2007; Sukro et al., 2013). Therefore the time-depth curves will probably be derived from data with a larger scatter than elsewhere in the study region. Ten wells were used in the analysis (Table 1), fewer than on the Labrador margin. The sonic log and checkshot data for some of the wells on the West Greenland side is not available, and neither is the quantitative systematic lithological analysis which allows the provisional separation of high velocity sandstones from other units in the Labrador region. We have included in this

region all the West Greenland wells where data has been released (Fig. 1; Table1), even though it could be argued that the northernmost of these lie within southern Baffin Bay.

3.1 Sonic logs

The logs for the Davis Strait wells required some editing to exclude depths where basalts are present, and to remove bad data. Otherwise the methods used are the same as Labrador, except that all lithologies were grouped together without any analysis of the possible role of compositional changes. Results for the Labrador margin suggest the regional data is not sufficient to support a more detailed approach. Figure 9 shows the sonic log data (see Table 3 for parameters of least squares fit). The time-depth curve derived from the sonic log data (Fig. 10, Table 4) lies between the Labrador 'high sandstone content' curve and Labrador 'all lithologies' curve.

3.2 Checkshot Surveys

Figure 10 also shows the checkshot data points for Davis Strait, compared to those for Labrador. The Davis Strait checkshots generally show more scatter than those for Labrador; and this greater spread starts at shallow depths, suggesting that the near surface velocities may exhibit more variation in the Davis Strait region. However, the overall trends of the two regional checkshot datasets are very similar. From about 0 to 3500 m, a single curve could be used to describe depth-time in both Labrador and Davis Strait, given the scatter in the data, and in fact the two polynomials show little divergence to about 5000 m depth.

Both sonic log and checkshot results for Davis Strait are compared (Fig. 10) with the Labrador checkshot function (Labrador 'all lithologies' sonic curve is not shown for clarity and because the results are almost identical to the Labrador checkshot curve). There is a very reasonable similarity between the Labrador and the Davis Strait checkshots, with a divergence of about 200 m at a depth of 5000 m. However, there is a much larger difference between the Davis Strait sonic logs and checkshots. At depths less than about 2500 m the sonic logs and checkshots give compatible results, similar to the Labrador data. However, the curves diverge markedly at deeper levels where the data is more limited in Davis Strait. Reasons for this are unclear, but may be a reflection of the sparse spatial sampling of the two datasets, which do not include exactly the same set of wells and therefore may emphasize different regions (Table 1). It would also be useful to have detailed lithological data as another major reason for the divergence of the two datasets may be due to variations in lithology. The checkshots and sonic logs differ in how they express lithological changes, so we might expect a divergence between the results where these changes are not considered

3.3 Wide-angle Seismic Data

We need to extend the depth-time conversion to greater depths in Davis Strait. The maximum sediment thickness in Davis Strait and southern Baffin Bay lies between 5 and 6 km, deeper than the datasets used above (Suckro et al., 2013; Funck et al., 2007). Also, since the sonic log and checkshot functions diverge at depths we need to establish which of these is the most realistic choice. Therefore we analyzed the available wide-angle seismic reflection/refraction data available in the Davis Strait region. This data has good resolution, better than that on the Labrador margin, with a close spacing of Ocean Bottom Seismometers and often a corresponding seismic reflection line along the profile. Velocity-depth data for the sediments from the three modern seismic refraction profiles in Davis Strait were analyzed and numerically integrated over depth to give time-depth curves (AWI line 20080700; Sukro et al., 2013; Nugget line 1, Funck et al., 2007;

Nugget line 2, Gerlings et al., 2009; see Fig. 1 for location). The velocity-depth data were analyzed at an average spacing of about 10 km along each of these seismic lines. This spacing varied somewhat between the profiles; the Nugget profiles provided a more irregular spacing of positions where velocities were specified, while the AWI 20080700 line was sampled at regular intervals of 10 km, and may therefore be more representative of the region. We have edited out all data below the sediments and within any basaltic layers as indicated by the published seismic interpretations along these profiles (see Appendix).

We have integrated the velocity-depth distributions at specific distances as described above along the seismic lines: $t = \int v(z)dz$. The resulting time-depth data plots are shown in the Appendix (Figs. A1 to A3) for each of these three lines separately. In each case the best fitting 2nd degree polynomial describing the time-depth function was derived. The data show scatter of about 300-400 m depth for a given time, which is similar to that of the checkshot data described above. All three of the derived time-depth functions lie within 200 m of checkshot data over the measured range of depths. Nugget 2, exhibit the greatest divergence from the checkshots where the sediment velocities were not well resolved (Gerlings et al., 2009). The discrete, stepwise nature of the time-depth data points for AWI 20080700 (Fig. A3) is caused by the digitization of the velocity-depth data at an interval of 0.1 km.

The data from all three seismic lines was merged and a regional time-depth function was derived for Davis Strait (Fig. 11, Table 4). This time-depth curve is compared to those from other datasets in Fig. 12. Refraction and checkshot curves diverge by less than 200 m, over the entire depth range, while sonic logs diverge from refraction results by more than 500m at 5000 m depth. Overall the checkshots and wide-angle seismic results are very similar, especially at greater depths, while all of these curves give similar results at depths shallower than about 2000 m, where data is more plentiful. Parameters of the fitted polynomials are listed in Table 4. Since two of three datasets give similar results and allow us to extend the data coverage to greater depths than otherwise, either the checkshot function or the refraction results are a good choice for time-depth conversions. This of course could be reconsidered when lithological variations are included in the analysis.

3.4 Predictions of depths versus measured depths in wells

To estimate the ability of the checkshot function to predict the depths, we compared the differences between these predicted depths and those measured at the wells. Like the Labrador margin (see section 2.4), we used the basement pick where possible, or the top of volcanics or an identifiable deep horizon within the sediments. These predictions are shown in Fig.12. The rms average difference between the predicted checkshot curve and measured depths for 7 wells is 205 m. Clearly there is some scatter and there remains a concern that not all the time-depth curves show consistency. Actually the sonic logs fit the well depths slightly better (rms average difference of 148 m) but we prefer the checkshot or seismic refraction results for depth conversion, given their similarity to each other and to the regional checkshot data on the Labrador margin.

4. BAFFIN BAY

4.1 Wide-angle Seismic Data

No exploratory well data was available in Baffin Bay for this study, other than ODP site 645, and at this site both sonic velocity logging and shipboard velocity measurements on cores were largely unsuccessful. (Srivastava et al., 1987). Therefore we used velocity-depth data from recent wide-

angle seismic experiments conducted in 2008 and 2010. While there are several other seismic datasets in the Baffin Bay region, which in some cases provide good measurements at crustal levels, the data is not in general well resolved within the sediments. In this analysis only this most recent data was used, with accurate positioning, dense sets of Ocean Bottom Seismometers and airgun shots, as well as detailed two-dimensional modelling of the travel times. Often there is also a coincident near-vertical seismic reflection profile, capable of distinguishing sediments from various types of basement. This is important because of the widespread occurrence of Tertiary basalts (e.g. Funck et al., 2012) and of pre-rift sediments (e.g. the Thule Group, Proterozoic age, e.g. Altenbernd et al., 2016) that exhibit similar velocities to the deepest Mesozoic/Cenozoic sediments. Data from these basalts or pre-rift sediments or any outcropping basement rocks, as defined by velocities above about 4.8 km/s, are eliminated from the analysis (see Appendix). The deeper Mesozoic sediments in the Melville Bay Graben also exhibit a higher velocity (Altenbernd et al., 2014; 2015), reaching a maximum of about 5 km/s at depths over 6 -7km. Such high velocities may suggest a change in lithology as well as compaction of sediments. Like the Bjarni Formation on the Labrador margin, if we knew their spatial distribution and thickness, we could divide the sediments into an upper and lower unit, with differing velocity distributions. However, we do not have this information at present. The depth to the basement in the Melville Bay Graben would be deeper by approximately 600m if a higher velocity layer (~5 km/s) were included, than the results presented here.

Six regional wide-angle seismic lines were used in Baffin Bay (profileAWI-20100300 (Altenbernd et al., 2016); profileAWI-20100200 (Altenbernd et al., 2014), profiles AWI-20100400 and AWI-20080500 (Suckro et al., 2012), profile AWI20100450 (Altenbernd et al., 2015), profile AWI-20080600 (Funck et al., 2012). Velocity-depth profiles were used at a spacing of about 10 km along each line; velocities are given every 0.1 or 0.2 km in depth, with respect to the sea floor. Each velocity-depth profile was numerically integrated to give time-depth profiles. These have been plotted for each profile, shown in the Appendix (Figs. A4 to A8). For some profiles, subregions were examined to determine if any regional trends in velocities could be observed along the profiles (e.g. deep versus shallow regions). While some differences do occur across the seismic profiles there was nothing that appeared to be geographically systematic, and they were mainly small differences compared to the general spread of the data points. In this study, division into subregions is not discussed further but there is probably more that could be done in future studies. The spread in values of depth on the depth-time plots varies from about 400 m (AWI 20100300; Fig. A8) to almost 1000 m (AWI 20080600; Fig. A5). We have already discussed some of the possible reasons for this in the Davis Strait section. All the data from these profiles is merged (Fig.13) and a 2nd degree polynomial in time-depth is derived using least-squares. In order to justify combining all these data, a comparison of the time-depth least-squares functions for each of the seismic lines separately is made (Fig.14). A very well-behaved and tight grouping of the results is obtained, with only about 250 m divergence between them out to at least 6 km depth. This depth range (i.e. 0 to 6 km) covers most of the Baffin Bay region. Parameters of the best fitting polynomial for the merged dataset is given in Table 4.

5. COMPARISON OF REGIONAL TIME-DEPTH CURVES

Finally, we compare the depth-time curves for all three regions: Labrador margin, Davis Strait and Baffin Bay (Fig.15) . For the Labrador margin we show the checkshot results only; the sonic log results are almost identical. We also show a time-depth curve, which was derived using more sonobuoy data in the deep-water Labrador Basin (Li et al., 2014). These two Labrador curves diverge by about 250 m over the upper 5000m depth range. However, our analysis using checkshots fit the deeper sedimentary (depths >6000m) data better than the Li et al.(2014) curve.

The fastest velocities are found in Baffin Bay. The total spread of the depth values, given by the various curves at a depth of 5000m, is 600m. Probably a significant part of this spread is real, rather than errors in measurements, and due to regional geological factors such as depositional sources, erosion, and lithological changes. Given the different datasets used and the geographic particularities of data location this is a satisfactory result. Parameters for all these final curves (except Li et al., 2014) are given in Table 4.

6. CONCLUSIONS

1. Both checkshots and sonic logs give consistent results in the Labrador Sea region, and checkshots can be extrapolated below the level of the wells to deeper parts of the sedimentary basins, showing results consistent with the depths to basement from wide-angle seismic data. The rms spread between predicted depth and measured depth at the wells is 128m.

2. Davis Strait results are more variable, especially between the checkshots and sonic logs. The geographic distribution of the datasets is probably partly responsible for this. Well log results are sparse and therefore somewhat suspect at depths greater than 3500 m. The checkshot and wide-angle seismic data show very similar behaviour, and therefore either of these time-depth curves could be used for depth conversion. These curves are also very similar to the Labrador checkshot time-depth function.The match between predicted depth from the checkshots and measured depth at the wells gives an rms error of 205 m.

3. In Baffin Bay, the recent five high resolution wide-angle seismic lines give a tightly grouped set of time-depth curves. The merged data yields a time-depth curve that suggests slightly higher sediment velocities than the favoured curves for Davis Strait or the Labrador margin.

4. The checkshots results for Labrador and Davis Strait, and the seismic refraction results for Baffin Bay lie within 500 m of each other at a depth of 5000m. Along with the sonic log results for Labrador, these are the most reliable time-depth curves. Polynomial constants describing the time-depth 2nd order polynomials to these datasets are given in Table 4.

5. It would to be desirable in principle to have separate time-depth functions for each lithology. However, results using the available data for the Labrador margin highlight the practical difficulties and uncertainties in implementing such an approach. On that margin it appears that the syn-rift Bjarni formation exhibits significantly higher sonic log velocities than other units, but only when the composition is mostly sandstone. This is not always the case as the lithology of the Bjarni is quite variable. Furthermore it is not possible to consistently identify its presence on seismic reflection data, and wide-angle refraction data does not indicate a high velocity layer at the base of the sediments. Other methods, such as using a variety of other well logs, might be useful in future studies to further investigate the role of lithology in defining sediment velocity.

ACKNOWLEDGEMENTS

I am grateful to GEUS for providing checkshot data for wells on the West Greenland margin. Thomas Funck and Deping Chian provided digital data for the wide-angle seismic profiles. Qingmou Li prepared some of the digital datasets .Kate Dickie provided the time-depth pairs at the wells, and provided some of the raw checkshot and sonic log data. .

REFERENCES

Altenbernd, T., Jokat, W., Heyde, I., and Damm, V., 2014. A crustal model for northern Melville Bay, Baffin Bay; Journal of Geophysical Research: Solid Earth, v. 119, no. 12, 2014JB011559. https://doi.org//10.1002/2014JB011559

Altenbernd, T., Jokat, W., Heyde, I., and Damm, V., 2015. Geophysical evidence for the extent of crustal types and the type of margin along a profile in the northeastern Baffin Bay; Journal of Geophysical Research: Solid Earth, v. 120, no. 11, p. 7337–7360. https://doi.org//10.1002/2015JB012307

Altenbernd, T., Jokat, W., Heyde, I., and Damm, V., 2016. Insights into the crustal structure of the transition between Nares Strait and Baffin Bay; Tectonophysics, v. 691 pt. A, p. 31–47. https://doi.org//10.1016/j.tecto.2016.04.001

Balkwill, H.R., and McMillan, N.J., 1990. Mesozoic-Cenozoic geology of the Labrador Shelf, Chapter 7 (Part 1); *in* Geology of the Continental Margin of Eastern Canada, Geology of Canada, no. 2, (ed.) M.J. Keen and G.L. Williams, p. 295-324, Geological Survey of Canada.

Chian, D., Louden, K.E., and Reid, I., 1995a. Crustal structure of the Labrador Sea conjugate margin and implications for the formation of nonvolcanic continental margins; Journal of Geophysical Research, v. 100, no. B12, p. 24239–24253. https://doi.org//10.1029/95JB02162

Funck, T. and Louden, K.E., 1999. Wide-angle seismic transect across the Torngat Orogen, northern Labrador: Evidence for a Proterozoic crustal root; Journal of Geophysical Research, v. 104, no. B4, p. 7463–7480. https://doi.org//10.1029/1999JB900010

Funck, T., Jackson, H.R., Louden, K.E., and Klingelhöfer, F., 2007. Seismic study of the transform-rifted margin in Davis Strait between Baffin Island (Canada) and Greenland: What happens when a plume meets a transform; Journal of Geophysical Research, v. 112, no. B4, B04402. https://doi.org//10.1029/2006JB004308

Funck, T., Gohl, K., Damm, V., and Heyde, I., 2012a. Tectonic evolution of southern Baffin Bay and Davis Strait: Results from a seismic refraction transect between Canada and Greenland; Journal of Geophysical Research, v. 117, no. B4, B04107. https://doi.org//10.1029/2011JB009110

Issler, D.R., 1987. Thermal and Subsidence History of the Labador Margin. Ph.D. thesis, Dalhousie University, Halifax, Nova Scotia, Canada. 235 p.

Issler, D.R. and Beaumont, C., 1987. Thermal and Subsidence History of the Labrador and west Greenland continental margins. *In* Sedimentary Basins and Basin Forming Mechanisms, edited by C. Beaumont and A.J. Tankard, Can. Soc. Petrol. Geol. Memoir 12, p. 45-69.

Issler, D.R., 1992. A new approach to Shale Compaction and Stratigraphic restoration, Beaufort-MacKenzie Basin and MacKenzie Corridor, Northern Canada. *Am. Assoc. Petrol. Geol*., 76, p. 1170-1189.

Li, Q., Shimeld, J., Dickie, K., Dehler, S.A., Mosher, D., and Desroches, K., 2014. Seismic velocity modelling, fixed point optimization, and evaluation of positioning uncertainty in the central Labrador Sea region: methods, a software tool, and an application; Geological Survey of Canada, Open File 7665, 98 p.

Raiga-Clemenceau, J., Martin, J.P., and S. Nicoletis 1988. The Concept of Acoustic Formation Factor for more accurate Porosity determination for Sonic Transit Time Data. *The Log Analyst*, v. 29, no. 1, p. 54-60.

Royden, L, and C.E. Keen 1980. Rifting Process and thermal Evolution of the Continental Margin of Eastern Canada determined from Subsidence Curves. *Earth and Planet. Sci., Letts*., 51, p. 343-361.

Srivastava, S.P., Arthur, M., Clement, B., et al. 1987. Proc. Initial Repts. (Pt. A), ODP, 105, Site 645. p. 61-52.

Suckro, S.K., Gohl, K., Funck, T., Heyde, I., Ehrhardt, A., Schreckenberger, B., Gerlings, J., Damm, V., and Jokat, W., 2012. The crustal structure of southern Baffin Bay: implications from a seismic refraction experiment; Geophysical Journal International, v. 190, no. 1, p. 37–58. https://doi.org//10.1111/j.1365-246X.2012.05477.x

Suckro, S.K., Gohl, K., Funck, T., Heyde, I., Schreckenberger, B., Gerlings, J., and Damm, V., 2013. The Davis Strait crust—a transform margin between two oceanic basins; Geophysical Journal International, v. 193, no. 1, p. 78–97. https://doi.org//10.1093/gji/ggs126

Table 1 Labrador Margin and Davis Strait Wells

DAVIS STRAIT REGION WELLS

Well Name and ID number	Basin	RT-m	Water Depth-m	Lat. degrees	Long. degrees		
1. AT2-1	NUUK	24.0	104.0	64.3569	-55.4262	-	c
2. GJOA G-37	SAGLEK	24.0	117.0	62.9412	-59.1069	s	-
3. HEKJA O-71	SAGLEK	12.5	350.8	62.1812	-62.9783	s	-
4. HELLEFISK-1	SISIMIUT	12.0	163.4	67.8782	-56.7371	s	c
5. IKERMIUT-1	SISIMIUT	13.0	447.5	66.9368	-56.5887	s	c
6. KANGAMIUT-1	KANGAMIUT	12.0	180.0	66.1505	-56.1881	s	c
7. NUKIK-1	NUKIK	24.0	104.0	65.5269	-54.7585	s	c
8. NUKIK-2	NUKIK	24.0	117.0	65.6320	-54.7648	s	c
9. QULLEQ-1	FYLLA	36.0	1152.0	63.8134	-54.4499	-	c
10.RALEGH N-18	SAGLEK	12.5	339.0	62.2993	-62.5478	s	c

LABRADOR SHELF REGION WELLS

Well Name and ID number	Basin	RT-m	Water Depth-m	Lat. degrees	Long. degrees		
11. BJARNI H-81	HOPEDALE	12.2	139.0	55.5081	-57.7015	s	c
12. BJARNI O-82	HOPEDALE	12.0	144.0	55.5300	-57.7096	s	c
13. CORTE REAL P-85	HOPEDALE	13.4	438.0	56.0802	-58.2023	s	c
14. FREYDIS B-87	HOPEDALE	12.5	178.6	53.9370	-54.7110	s	c
15. GILBERT F-53	SAGLEK	12.1	183.0	58.8741	-62.1397	s	-
16. GUDRID H-55	HOPEDALE	12.2	299.3	54.9083	-55.8752	s	c
17. HERJOLF M-92	HOPEDALE	26.8	139.0	55.5314	-57.7479	s	c
18. HOPEDALE E-33	HOPEDALE	12.8	549.9	55.8734	-58.8479	s	-
19. INDIAN HARBOUR M-52	HOPEDALE	29.9	197.8	54.3642	-54.3977	s	c
20. KARLSEFNI A-13	SAGLEK	12.2	174.7	58.8708	-61.7783	s	c
21. LEIF M-48	HOPEDALE	12.2	165.2	54.2960	-55.1222	s	-
22. NORTH BJARNI F-08	HOPEDALE	12.5	150.0	55.5914	-57.7637	s	c
23. NORTH LEIF I-05	HOPEDALE	12.0	144.0	54.4108	-55.2529	s	c
24. OGMUND E-72	HOPEDALE	12.8	156.2	57.5249	-60.4438	s	c
25. ROBERVAL C-02	HOPEDALE	13.7	276.0	54.8522	-55.7679	s	c
26. ROBERVAL K-92	HOPEDALE	12.5	268.5	54.8598	-55.7432	s	-
27. RUT H-11	SAGLEK	11.6	124.0	59.1712	-62.2797	s	-
28. SNORRI J-90	HOPEDALE	11.3	140.8	57.3290	-59.9623	s	c
29. SOUTH HOPEDALE L-39	HOPEDALE	12.0	580.	55.8090	-58.8468	-	c
30. SOUTH LABRADOR N-79	HOPEDALE	11.3	449.9	55.8125	-58.4424	s	
31. TYRK P-100	HOPEDALE	12.3	117.0	55.4971	-58.2307	s	c
32. LEIF E-38	HOPEDALE	12.2	167.6	54.2916	-55.0967	s	-
33. POTHURST P-19	SAGLEK	12.0	193.0	58.8149	-60.5246	s	-
34. SKOLP E-07	SAGLEK	12.0	166.5	58.4403	-61.768	s	-

RT is the height of the rotary table above sea level in m
c=checkshot available, s=sonic log available
From Natural Resources Canada, Geological Survey of Canada, Geoscience Data Repository, BASIN Database

Table 2
The Labrador well data showing depth intervals and lithology.
Two groups defined by formation: sandstones and fine-grained lithologies (see text)

All fine-grained intervals used of Mokami, Kenamu,Cartwright and Markland Formations

Well ID	zmin-m	zmax-m	%shale
11	573.3	1998.8	99
12	602	2129	96
14	297.9	1195.9	88
14	1229.9	1268.9	82
14	1300.9	1538.9	96
15	966.9	2257.9	95
15	2263.9	2999.9	86
16	410.5	1867.5	97
16	2079.5	2351.5	96
17	607.7	2448.2	99
19	266.3	3022.3	77+
20	539.1	2004.1	80+
20	3584.1	3942.1	95
21	410.6	1079.6	85+
21	1121.6	1488.6	96
21	1517.6	1661.6	97
22	694.5	2260.5	94
25	413.3	1906.3	84+
25	2193.3	2503.3	97
30	310.8	3065.8	94+
13	1031.6	3717.6	88+
13	3736.6	4000	98
18	1135.3	1385.3	71
28	844.9	2339.9	nd
23	392	1319	91
23	2068	2566	92
24	807	1289	81+
27	1186.4	4314.4	70+
29	955	1328	83+
31	519.7	1064.7	84+

All sandstones of Saglek and Bjarni Formations, Gudrid, Leif and Freydis Members

Well ID	zmin-m	zmax-m	%sand
13	276.6	1031.6	44
18	50.3	277.3	nd
32	24.2	416.2	30
28	114.9	844.9	40

23	163	392	61
24	157	807	41
33	157	1244	34
26	59	444	nd
27	113.4	1186.4	71
34	171.5	508.5	0
29	38	220	nd
11	70.8	573.3	88
12	106	602	97
14	1195.9	1229.9	98
15	107.9	966.9	77
16	91.5	410.5	91
17	73.2	607.7	98
19	6.4	266.3	79
20	100.1	539.1	95
21	24.6	410.6	49
22	99.5	694.5	95
25	85.3	413.3	86
30	85.8	310.8	92
11	1998.8	2104	74
12	2129	2650	78
17	2448.2	3585.2	79
22	2660.5	2700	85
18	1385.3	1414.3	69
14	1538.9	1596.9	94
31	242.7	519.7	90
28	2871.4	2996.4	19
23	2566	3238	61
24	2671	2776	41
26	2799	2907	52
34	2294.5	2789.5	24
29	1328	1415	8
31	1064.7	1393.7	10
30	3065.8	3086.8	49
14	1596.9	1713.9	37
14	1195.9	1229.9	97
14	1538.9	1596.9	94
16	1867.5	2079.5	98
23	1406	1432	85
23	1985	2068	80
24	1289	1371	88
25	1906.3	2193.3	99
34	759.5	807.5	72

All data from BASIN Database. Well ID numbers as in Table 1. All depths in metres.
zmin and zmax give the depth range of interval with depths measured from seafloor.
% sand or shale from CanStrat logs.

Table 3. Parameters k and l obtained from least squares fit of sonic log transit time data, where $dt-dt_{ma}=kexp(-lz)$ (see text)

Region/dataset	k in μseconds/m	l in 1./m
Labrador all lithologies dt_{ma}=222 μseconds/m	313.3	0.0004484
Labrador sands dt_{ma}=182	368.97	0.0005699
Davis Strait all lithologies dt_{ma}=222	312.69	0.0005884

Table 4. Final Results. Parameters describing the time-depth conversion functions for various datasets.

Region / dataset	a	b	c
Labrador all lithologies-sonic logs	9.076	1779.96	634.21
Labrador sand only-sonic logs	29.307	1543.34	1136.006
*Labrador checkshot surveys-all lithologies	-14.562	1983.422	502.628
Davis Strait all lithologies-sonic logs	-1.01797	1822.472	800.247
*Davis Strait checkshot surveys	-18.389	2101.922	381.189
Davis Strait wide-angle (Nugget1 and 2 and AWI-20080700)	-16.853	1766.21	585.583
*Baffin Bay all wide-angle seismic lines	-39.728	2037.081	579.745

Note: . The time-depth functions are described by 2nd order polynomials: $z=a+bt+ct^2$, where z in metres and t one-way travel time in seconds. * denotes preferred functions.

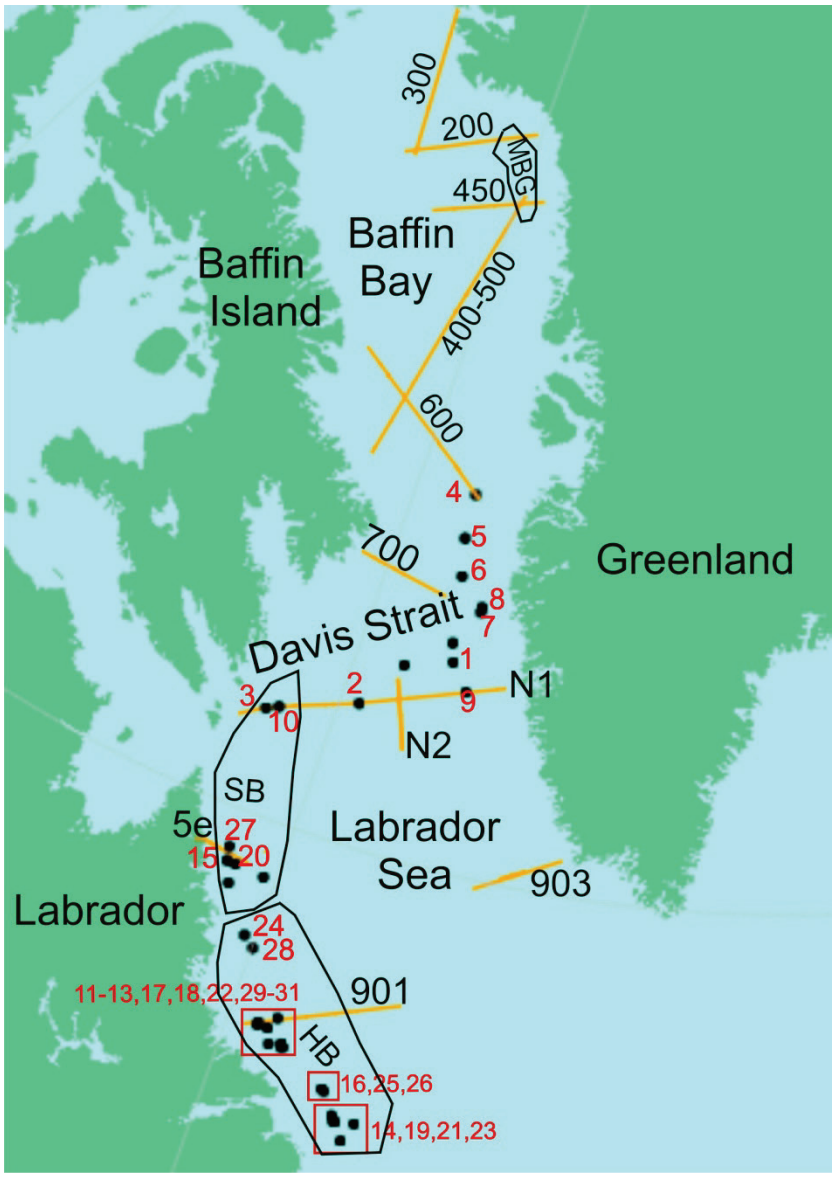

Figure 1. Location map showing seismic lines (orange) and wells (black dots) referred to in the text. Lettering in black refers to seismic refraction lines: N1 and N2 refer to the Nugget1 (Funck et al., 2007) and Nugget 2 (Gerlings et al., 2009) lines; '901' refers to line 90R1 of Chian et al. (1995); numbers, '200' to '700' refers to lines AWI 20100200 (Altenberndt et al., 2014); AWI 20100300 (Altenberndt et al.,2016) ; AWI 2010450 (Altenberndt et al., 2015); AWI 20100400 (Suckro et al.,2012) ; AWI 20080500 (Sukro et al., 2012); AWI 20080600 (Funck et al., 2012); AWI 20080700 (Suckro et al., 2013); and '5e' is line ECSOOT line 5e (Funck and Louden, 1999). Numbers in red beside wells are cross-referenced to Table 1 which lists the well names and basic parameters. Wells not labelled are not used in the analysis. Groups of wells are indicated by red boxes, with numbers referring to the wells included in the box. 'HB', 'SB' and 'MBG' refer to the Hopedale Basin, Saglek Basin and Melville Bay Graben, respectively. Rough outlines of these basins are also shown.

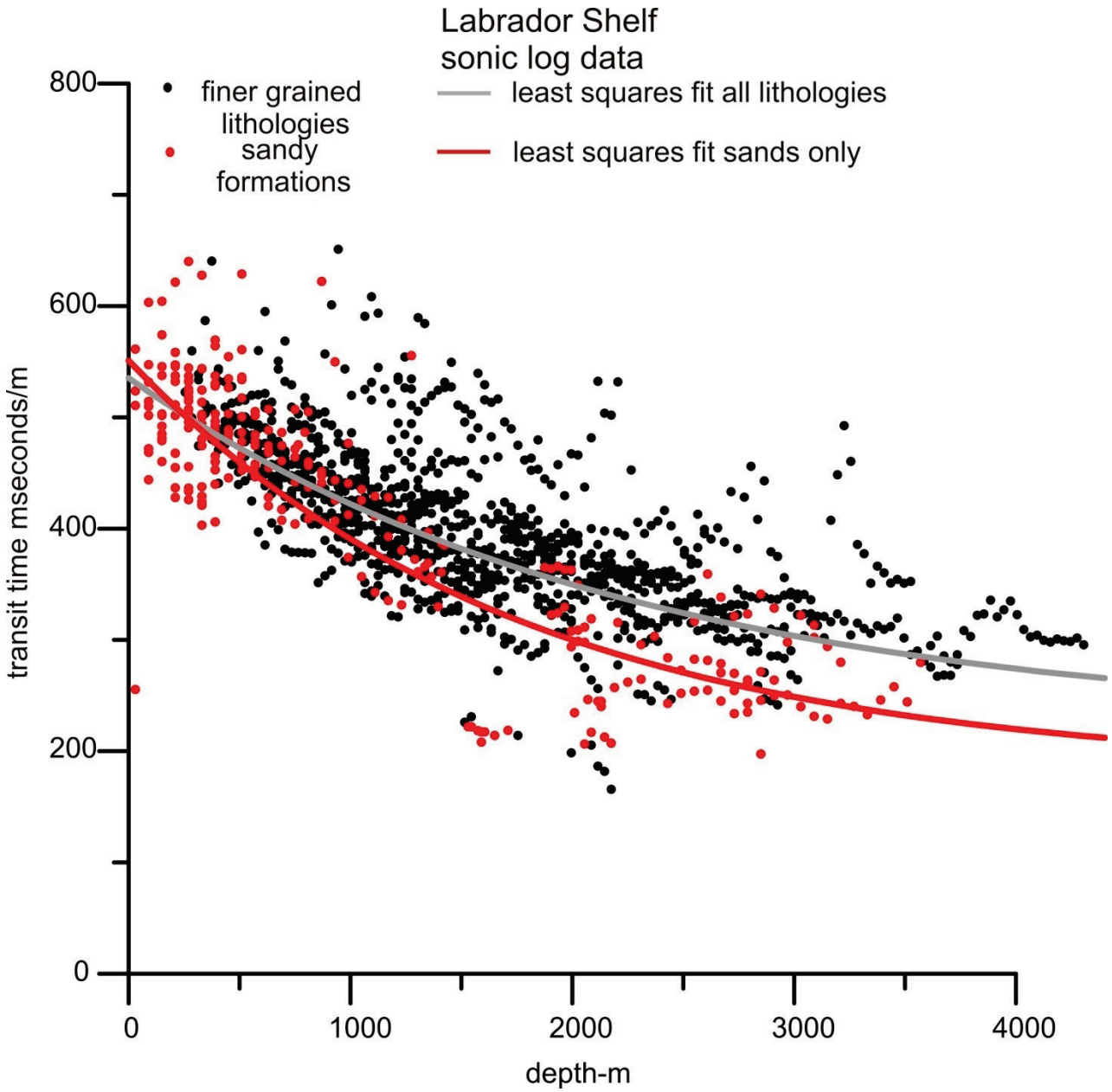

Figure 2. Labrador margin sonic logs for 20 wells. Plot of dt (transit time in µsec/m) vs depth (m). All depths are measured from the sea floor. They have been divided into two groups indicated by the black and red dots, on the basis of Formation. Red circles indicate that the composition is nominally sandstone, while black dots include all finer grained lithologies. See Table 1 for wells used. Solid lines are least squares fits to the data as described in the text; grey line corresponds to for finer grained lithologies and red line to sandy lithologies. The relationship used is $dt=dt_{ma}+kexp(-lz)$, where dt_{ma} =matrix transit time (222 µsec/m for shale, 182 µsec/m for sands, see text). The fitted values of parameters k and l are shown in Table 3.

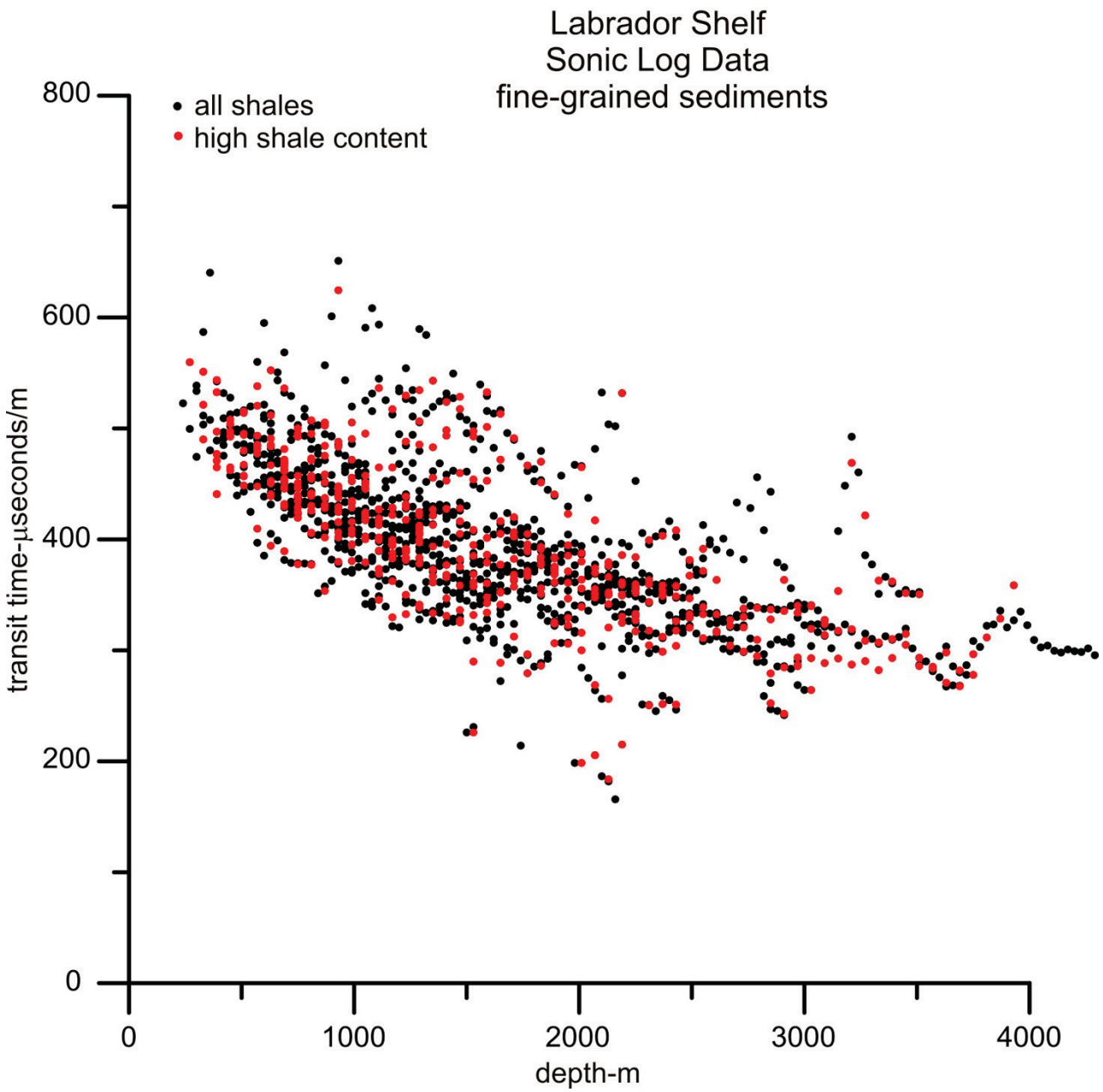

Figure 3. Labrador margin sonic logs. dt versus depth below sea floor for fine grained formations as described in the text (section 2.1). Red dots are data for which shale %>80 , from CanStrat logs (Table 2). Black dots are all other shale formations.

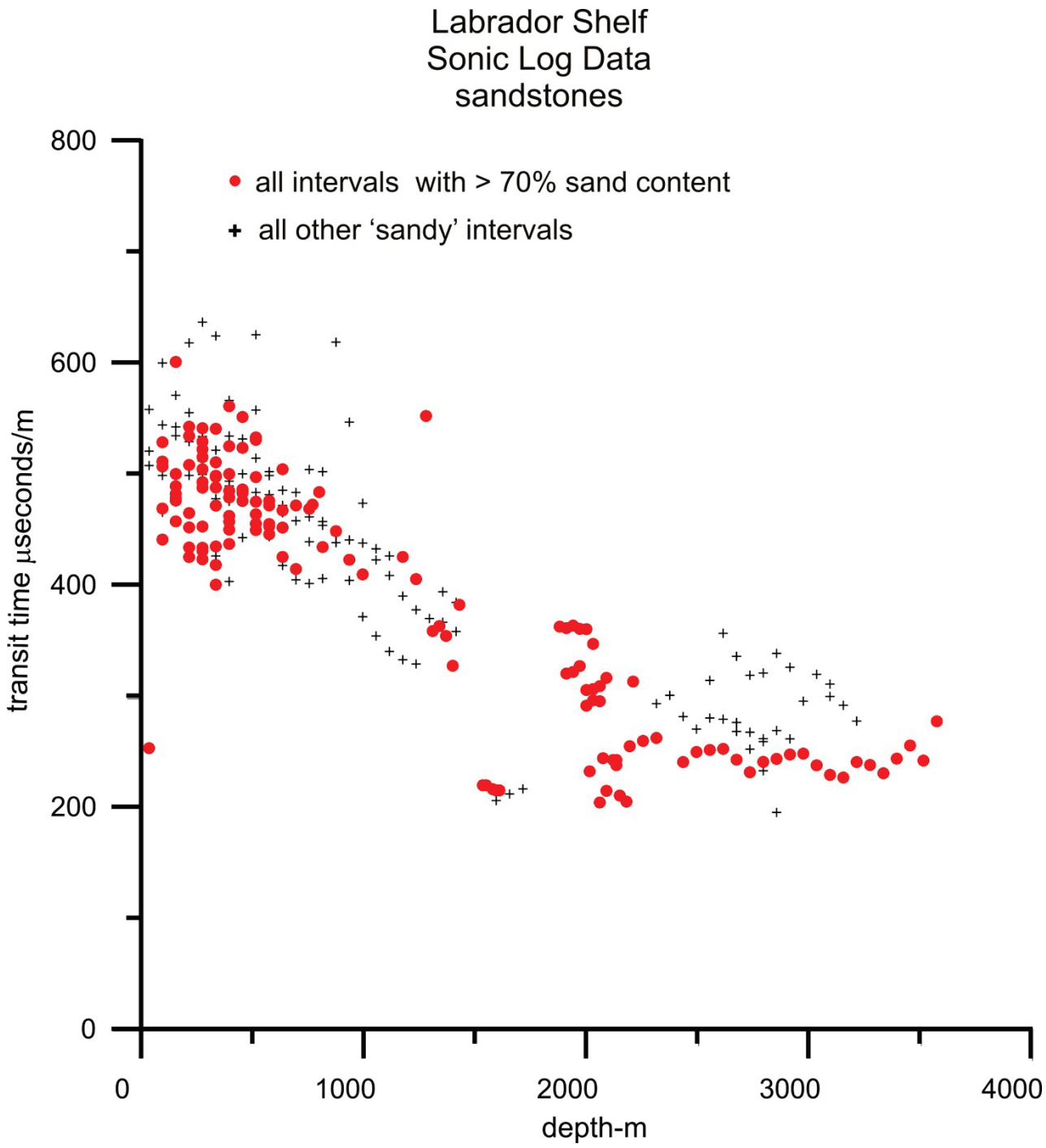

Figure 4. Labrador margin sonic logs, transit time dt versus depth below sea floor for sandstone units as described in the text. Black crosses are all sandstone formations regardless of actual sand content. Red are points for which sand%>70, according to CanStrat logs (Table 2).

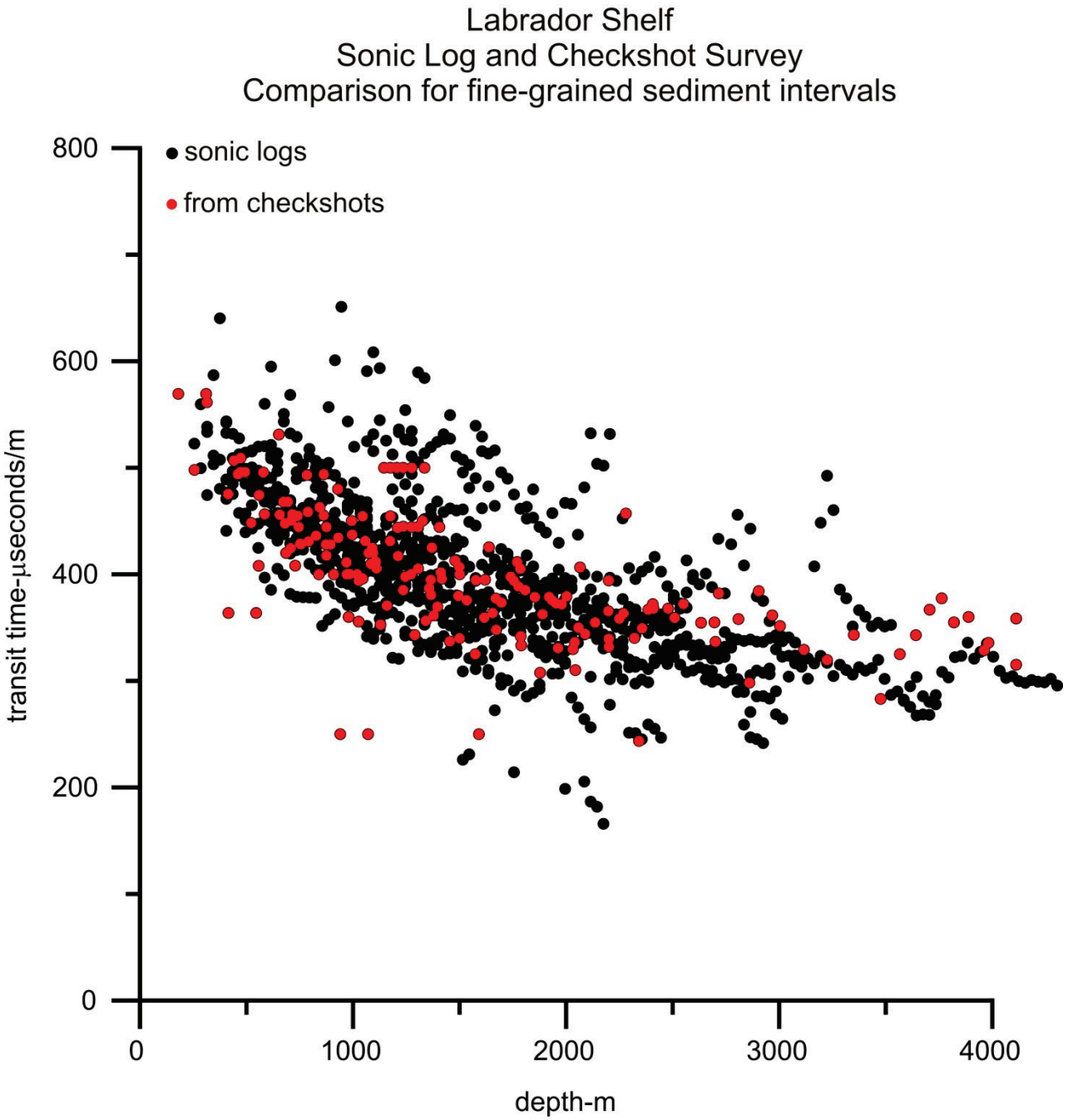

Figure 5. Comparison of Labrador margin checkshot surveys (red dots) with sonic logs (black dots) for all fine-grained formations. The checkshot data was differentiated with respect to depth to obtain proxy transit times.

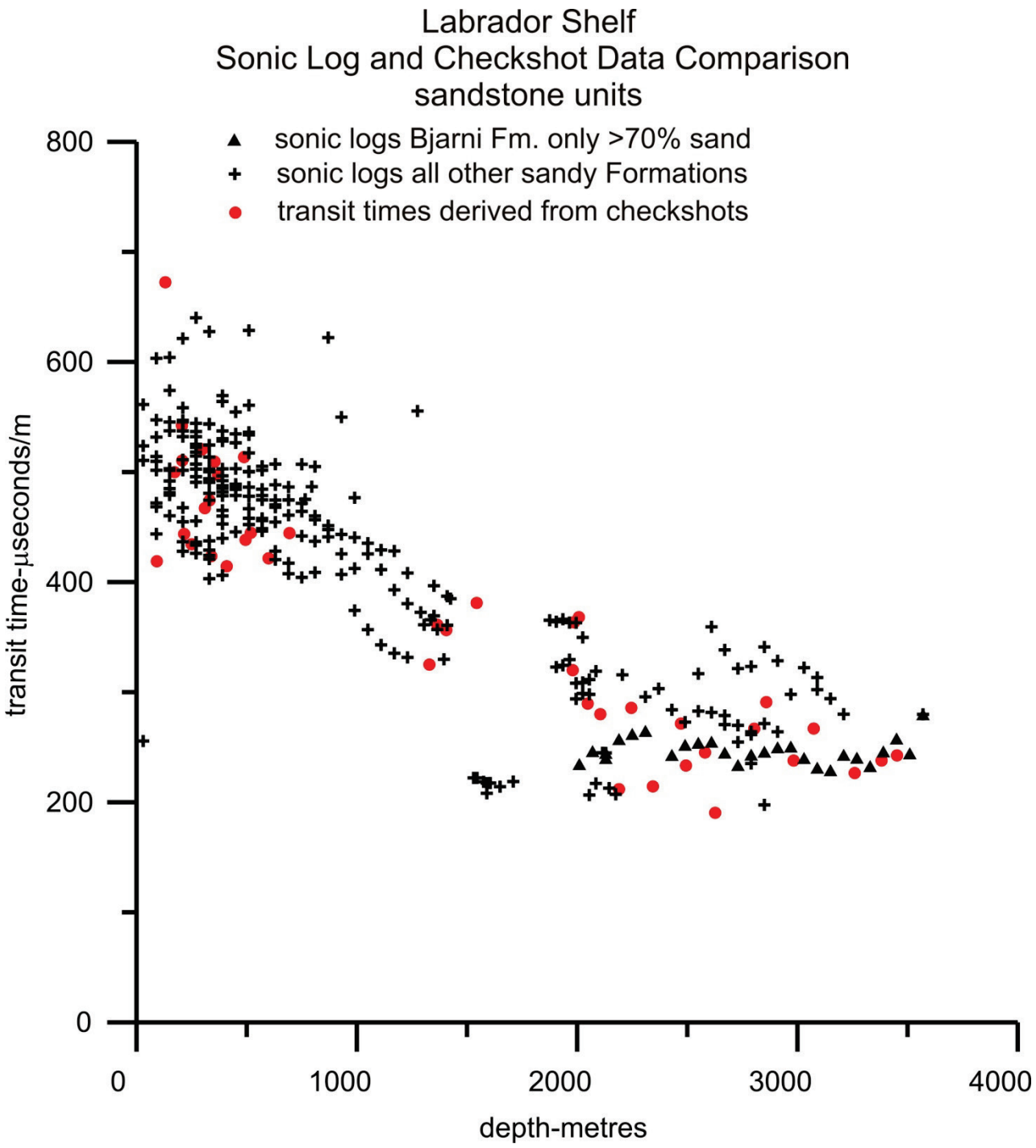

Figure 6. Comparison of Labrador margin checkshot surveys (red dots) with sonic logs (crosses) for sandstone Formations. The Bjarni Formation sonic log picks with sand content over 70% are shown as black triangles.

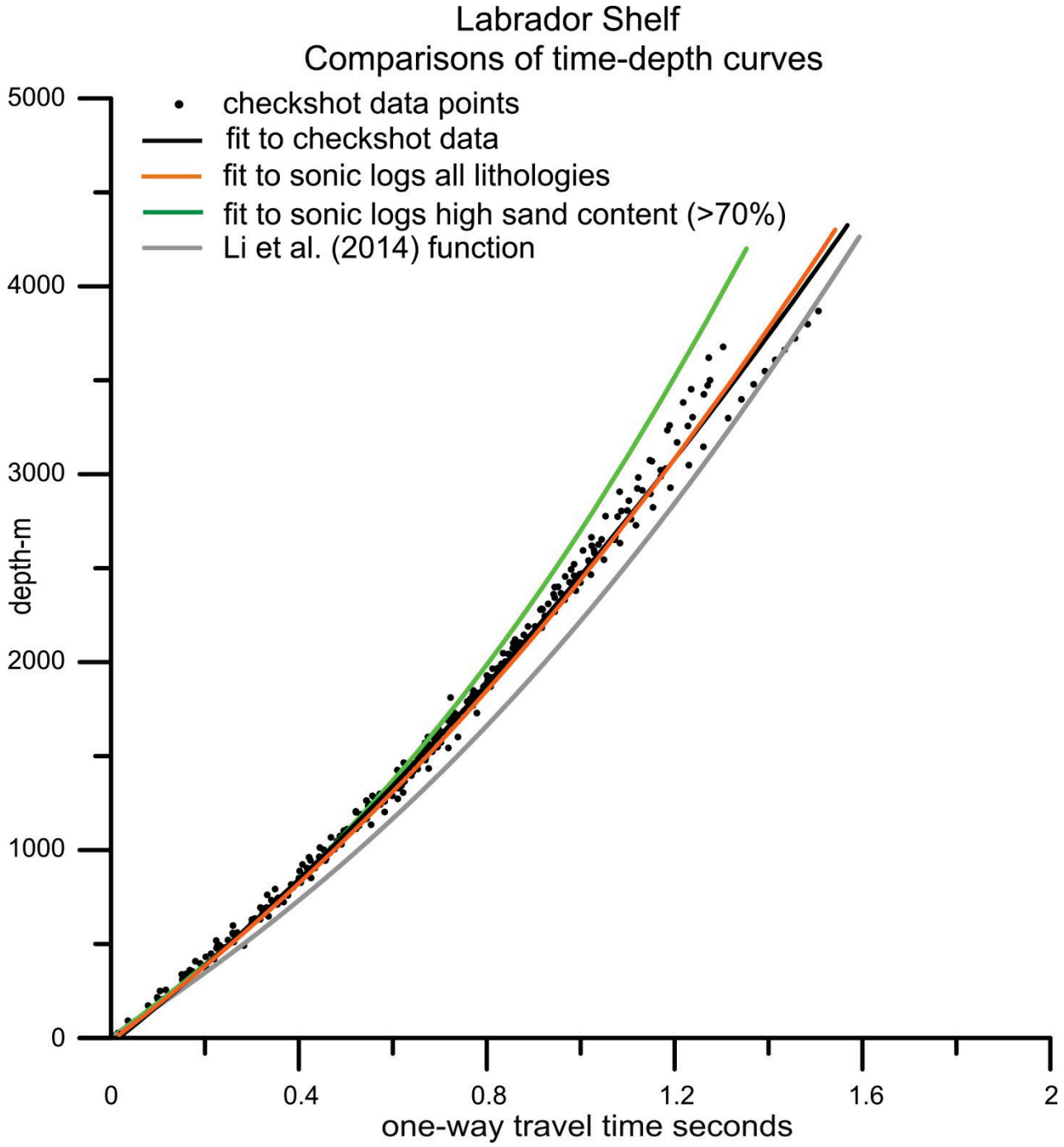

Figure 7. Depth-time results from Labrador checkshot surveys for 15 wells (black dots), and resulting least squares fits (black line). The 2nd order polynomial coefficients defining this line are shown in Table 4. The time-depth curves derived from the sonic logs are also shown; for all lithologies (orange) , as well as for high sand content units (green). The grey curve is the depth-time curve derived by Li et al. (2014) for the Labrador Sea region and includes more deep-water seismic data.

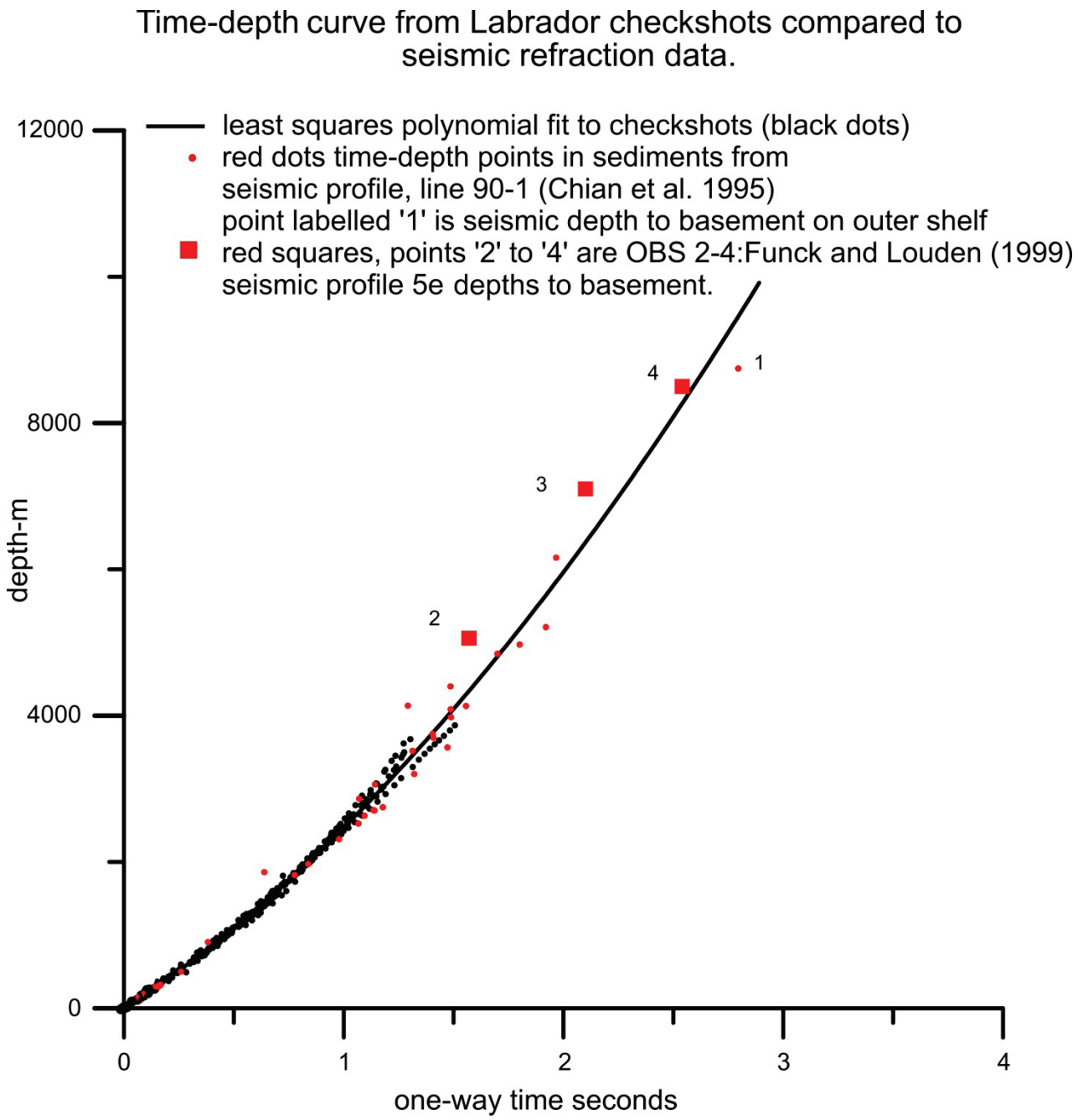

Figure 8. Extrapolation of depth-time results from Labrador checkshots, showing the relationship to the seismic refraction time-depth pairs from results of Chian et al (1995) (line 90-1, red dots) and Funck and Louden (1999) (line 5e, OBS 2 to 4, red squares). Black line is least squares time-depth function for checkshot data (black dots). Red dots are time-depth from wide-angle seismic data on line 901 (Fig. 1, Chian et al., 1995). Dot labelled "1" is the basement on the outer Labrador shelf. Red squares "2" to "4" are basement at OBS seismic stations 2 to 4 on line 5e (Fig. 1, Funck and Louden, 1999).

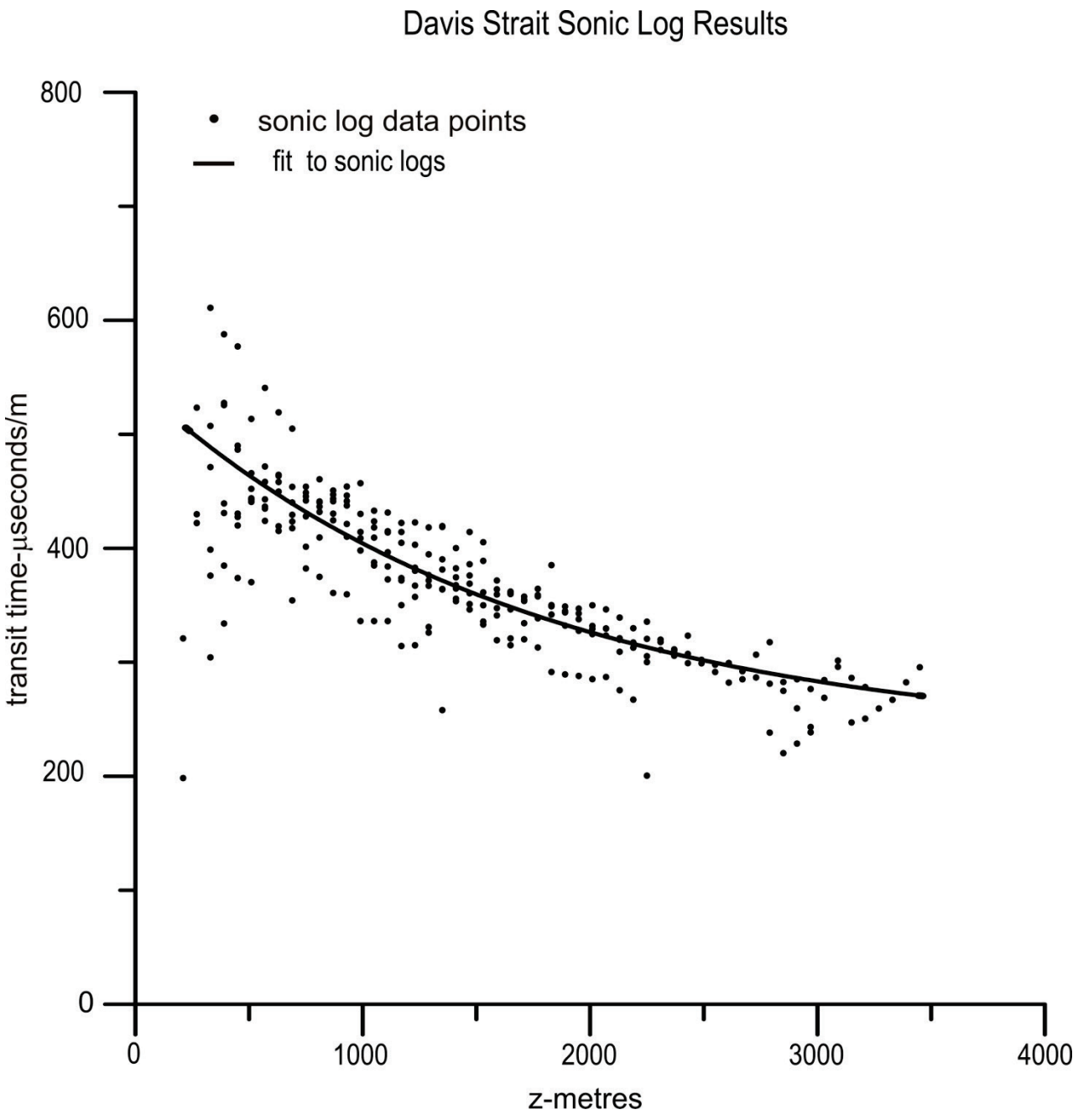

Figure 9. Davis Strait sonic log results (black dots) with a least squares fit to $dt=dt_{ma}+kexp(-lz)$ (black line). Parameters k and l are listed in Table 3.

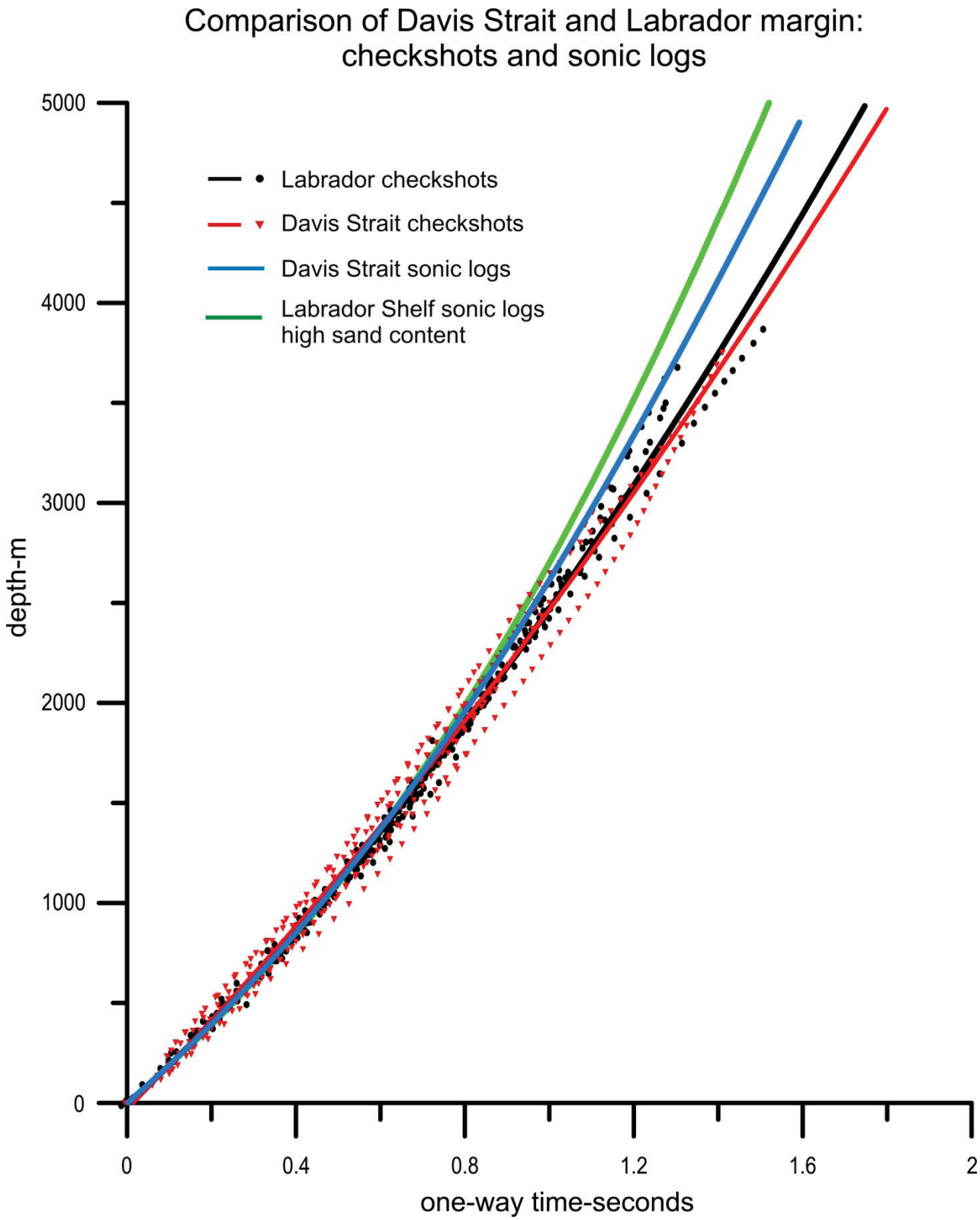

Figure 10. Comparison of time-depth checkshot data from Labrador and Davis Strait. See Table 1 for wells used and Table 4 for the least squares best fitting polynomials. Black dots are Labrador checkshots and red triangles are Davis Strait checkshots. Sonic log results are shown for the Labrador margin high content sandstone units (green), and for Davis Strait (blue line).

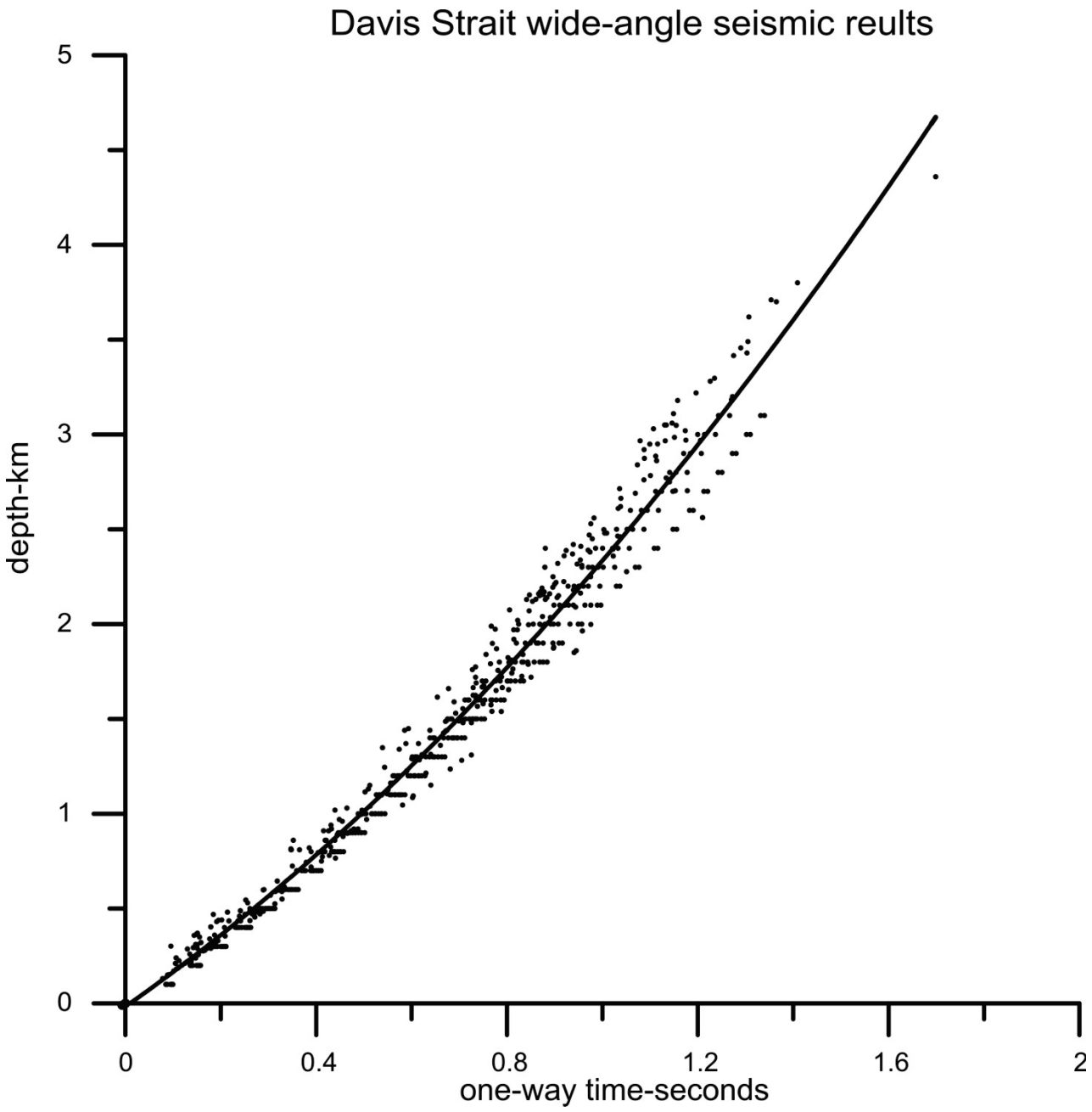

Figure 11. Merged wide-angle seismic data from Davis Strait, including Nugget lines 1 and 2 and line AWI20080700. Best fitting least squares polynomial is shown (black line).

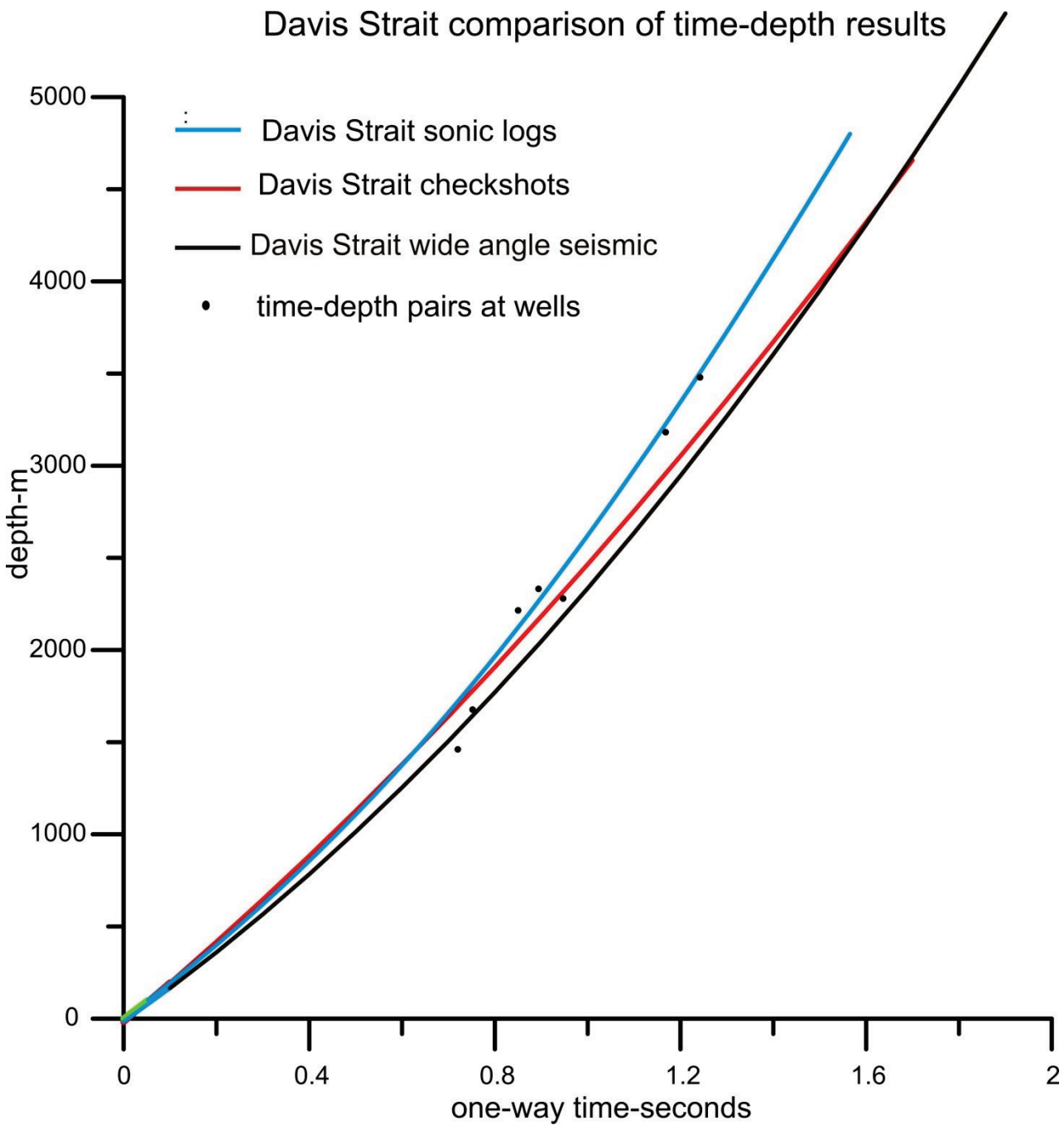

Figure 12. Time-depth functions for Davis Strait, from sonic log, checkshot and wide-angle seismic datasets. The time-depth pairs at selected wells, where basement or other deep horizons were sampled are shown.

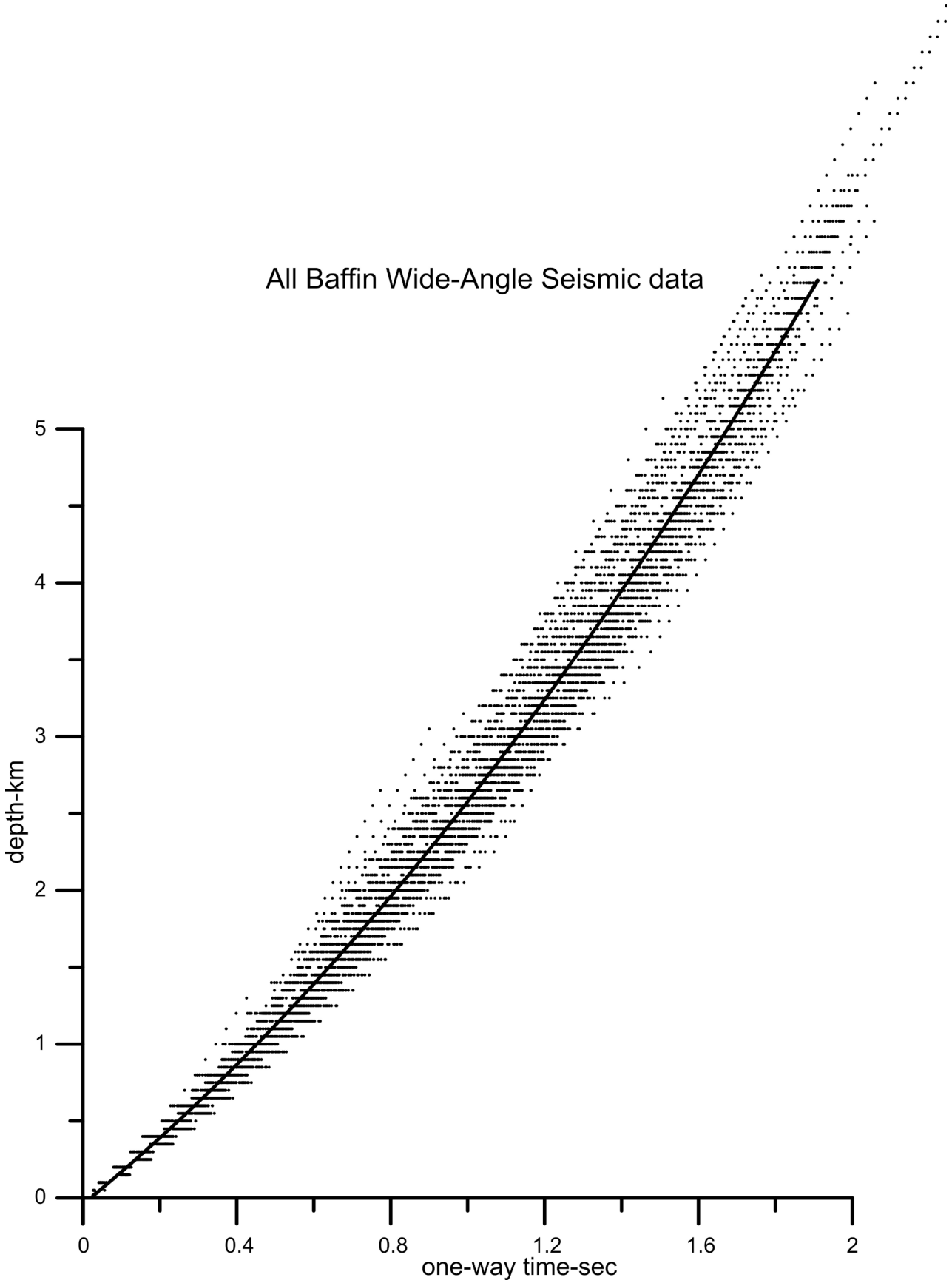

Figure 13. All Baffin Bay time-depth results created by merging data from all wide-angle seismic lines (see Table 4 and 5), with the best fitting polynomial (black line).

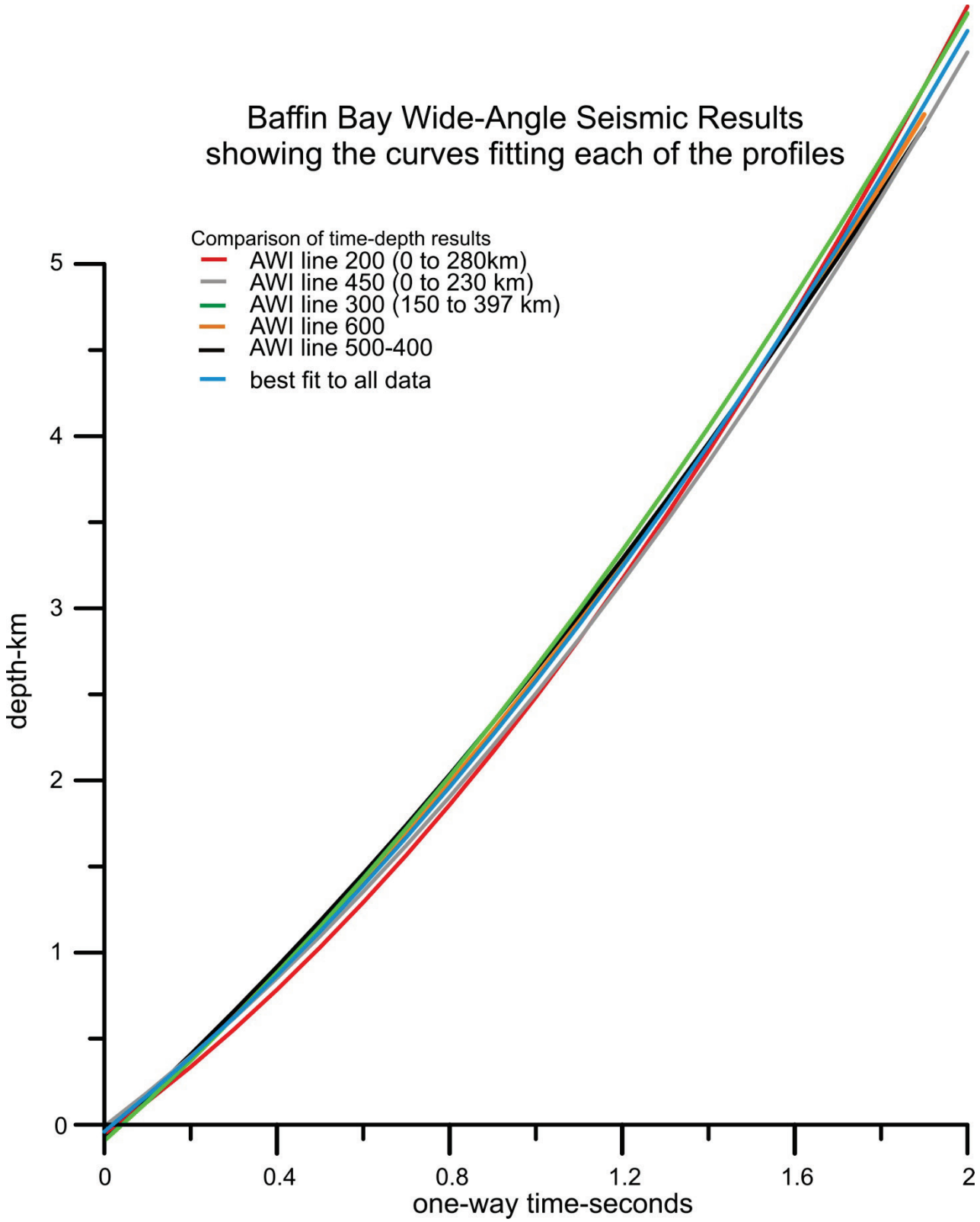

Figure 14. Comparison of time-depth curves for Baffin Bay for each of the 5 seismic profiles separately and for the merged dataset.

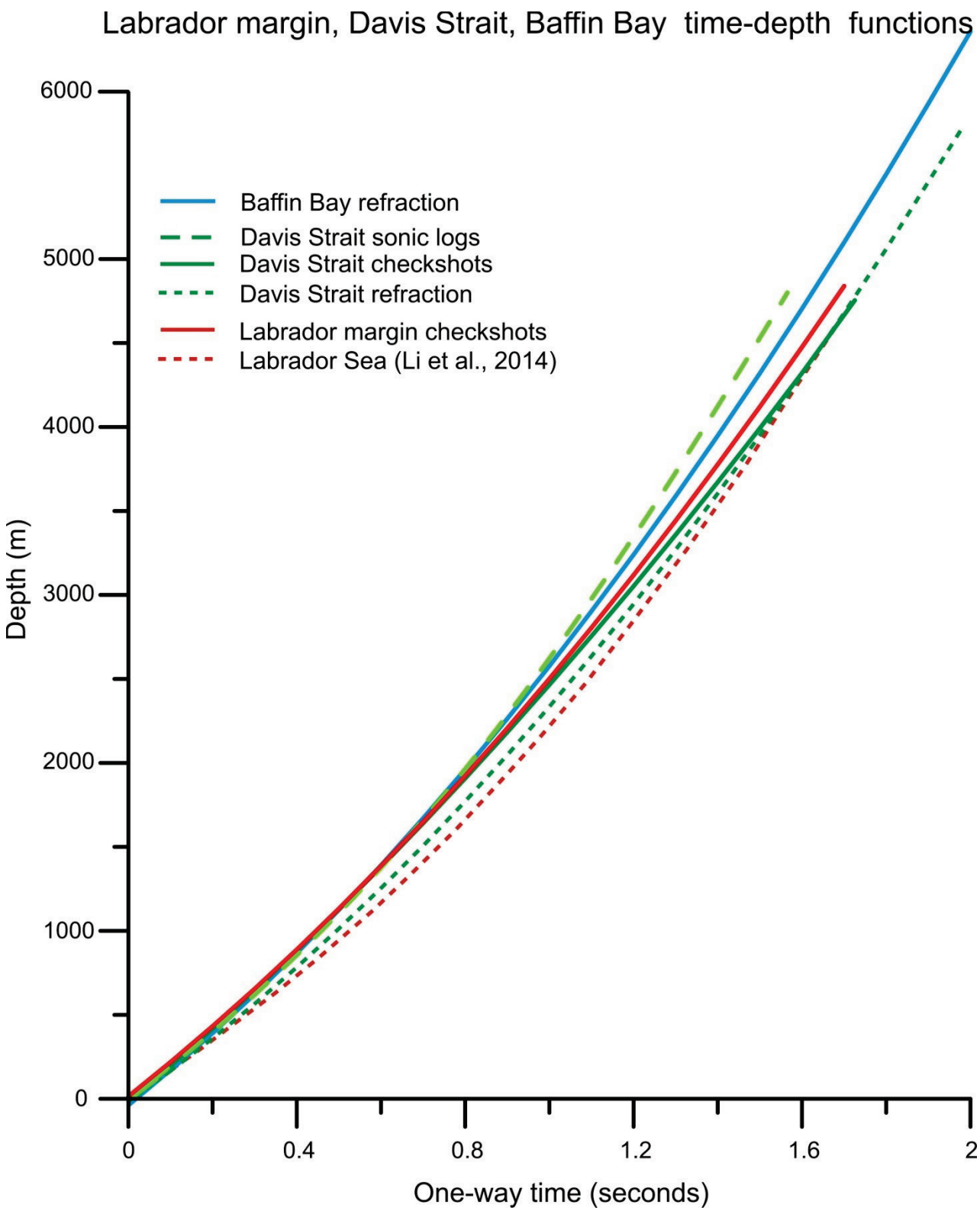

Figure 15. Comparison of depth-time curves for Baffin Bay, Davis Strait, and Labrador Sea. See legend for details.

APPENDIX

In Baffin Bay and Davis Strait most of the data along wide-angle seismic lines[1] was used in the analysis, exceptions are listed below.

AWI-20100200 used from 0 to 280 km of model, (with 190 to 210 km excluded due to basement high)
AWI-20100300 used from 150 to 397 km of model (not further north, where results are modified by Thule group Proterozoic sediments)
AWI-20100450 used from 0 to 230 km (not further east, on basement)
AWI-2010 0400 used whole profile
AWI-20080500 used whole profile
AWI-20080700 used whole profile.
Nugget 1 used whole profile
Nugget 2 used from 0 to 102 km of model ('continental' part in Davis Strait)

---

[1]see also Figs. A1 to A8 in this Appendix.

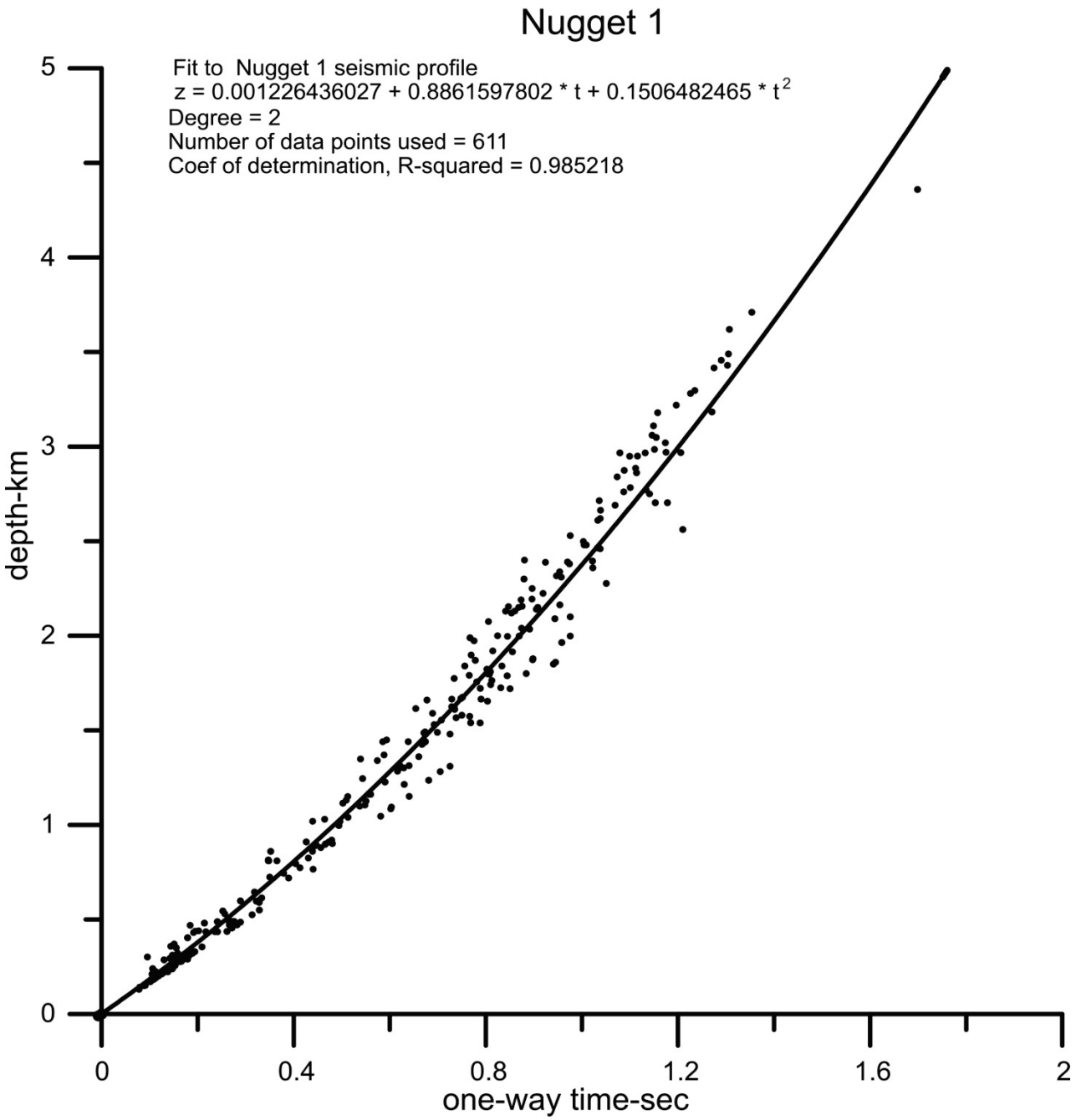

Figure A1. Depth vs time curves from the Nugget1 seismic profile in Davis Strait (Funck et al., 2007). The polynomial fit to the data is shown (black line).

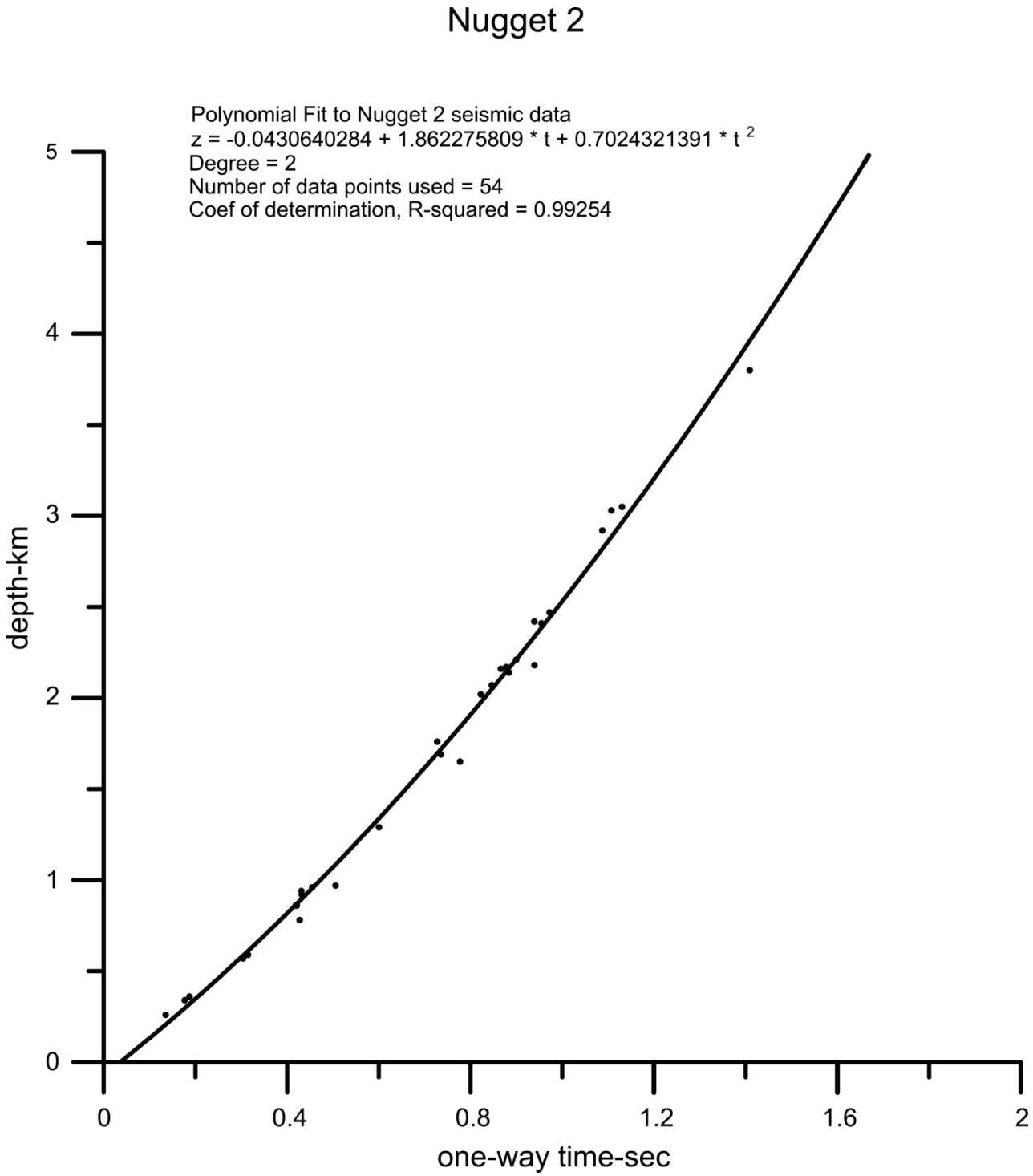

Figure A2. Depth vs time from Nugget line 2 (Gerlings et al., 2009). The polynomial fit to the data is shown (black line).

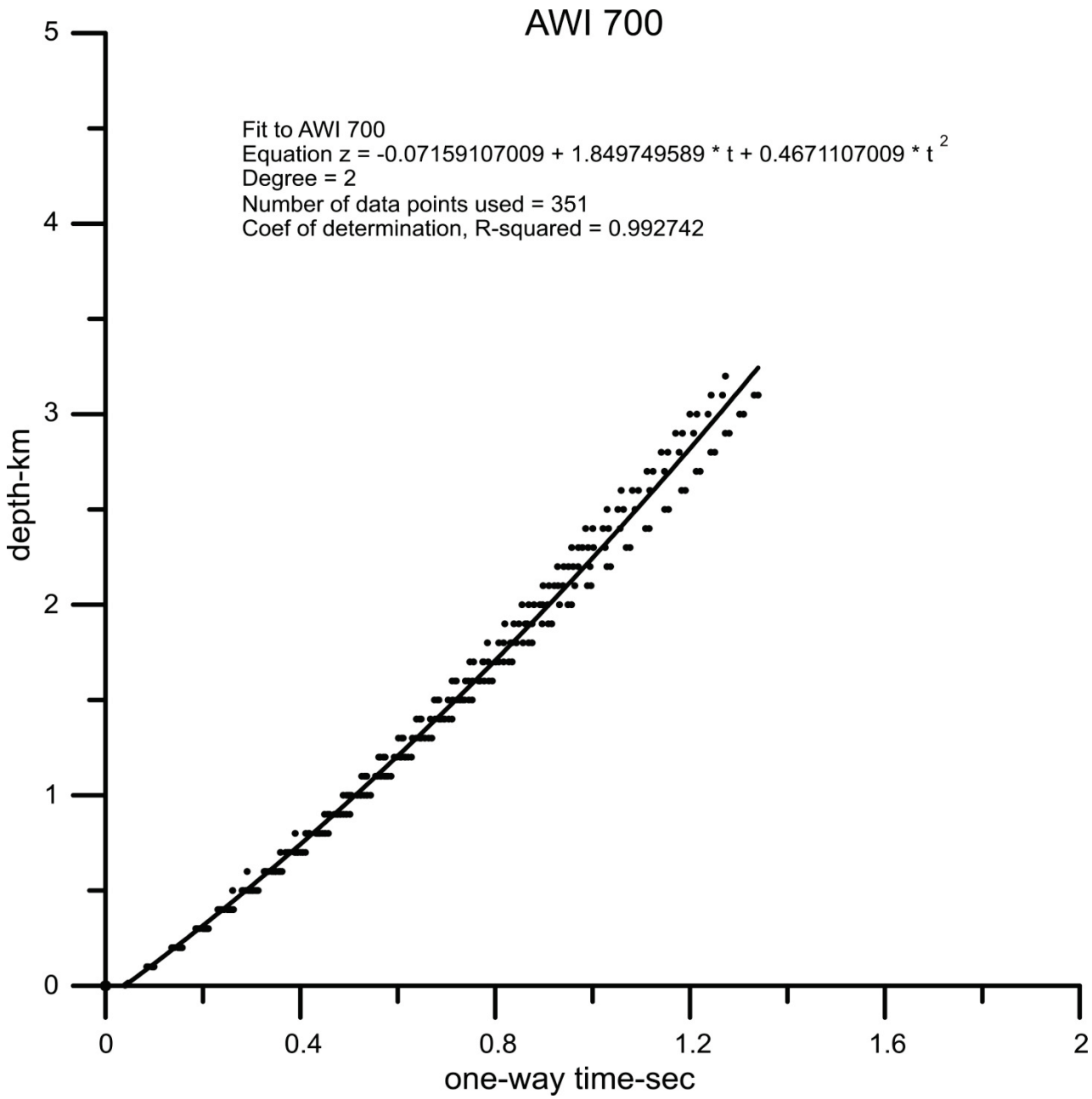

Figure A3. Depth vs time curves from the AWI-20080700 seismic profile in Davis Strait (Sukro et al., 2013). The polynomial fit to the data is shown (black line).

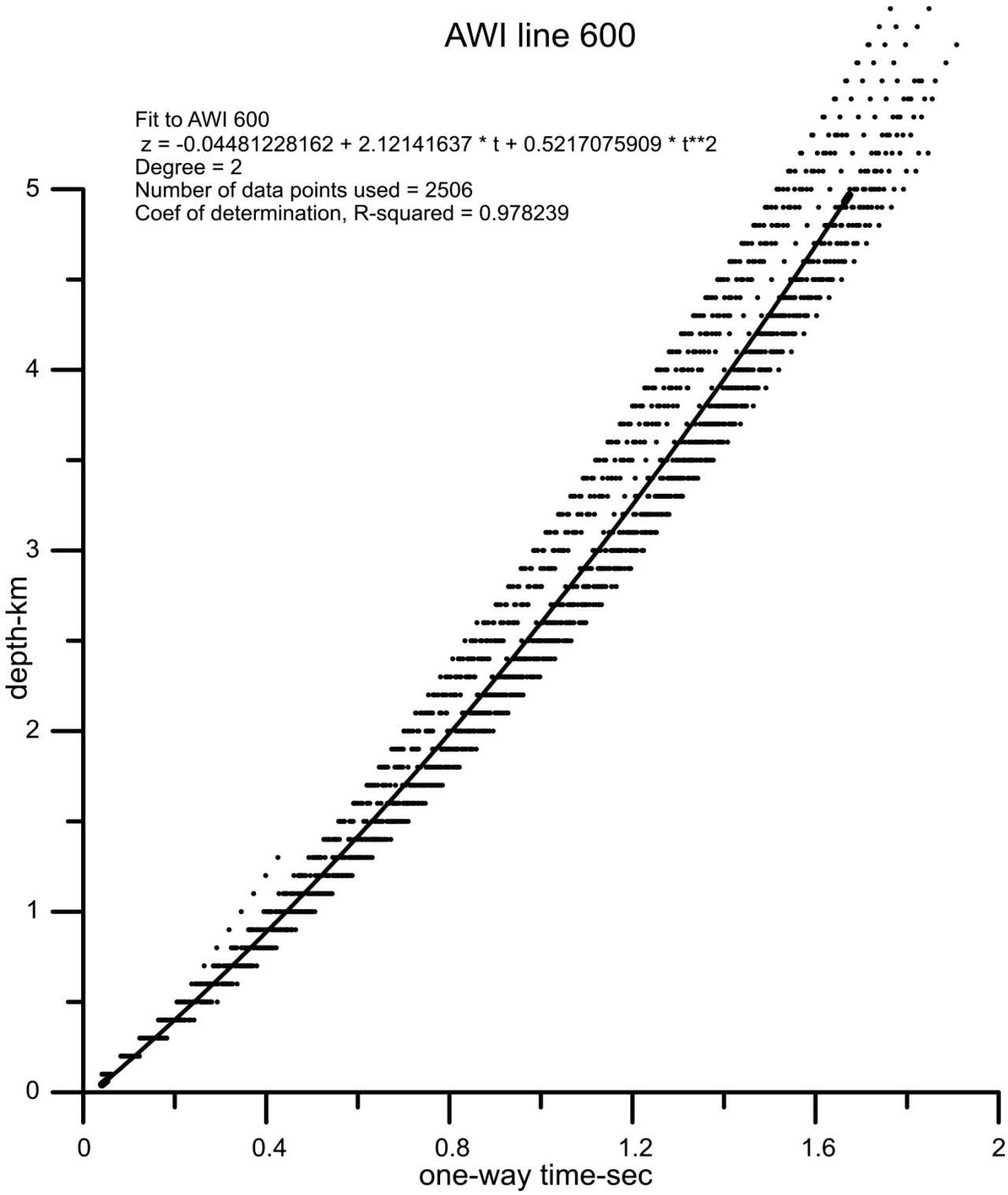

Figure A4. Depth vs time curves from the AWI-20080600 seismic profile in southern Baffin Bay (Funck et al., 2012). The polynomial fit to the data is shown (black line) . Note change of vertical scale here to kilometers.

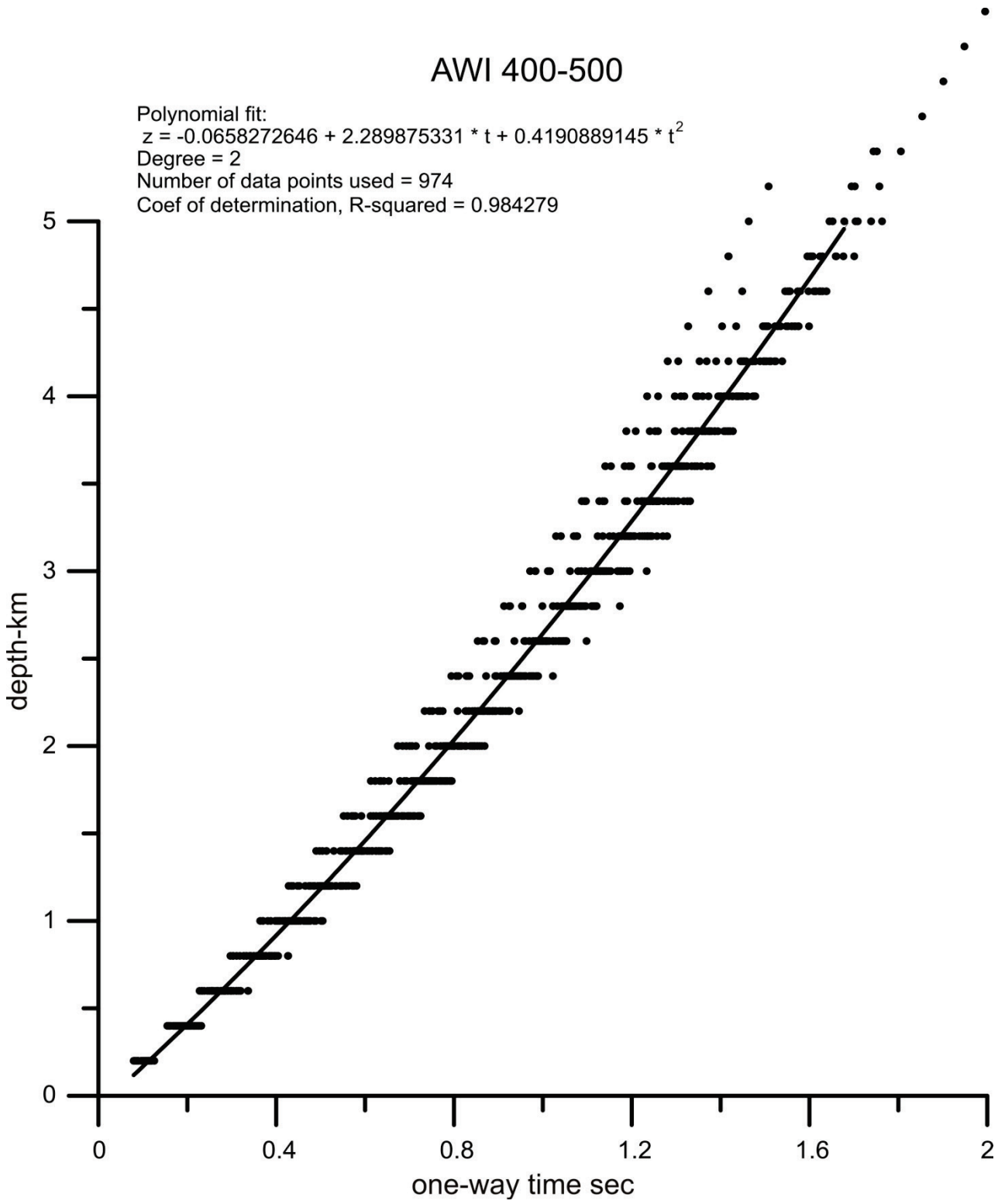

Figure A5. Depth vs time curves from the AWI-20080500-20100400 seismic profile in southern Baffin Bay (Sukro et al., 2012). The polynomial fit to the data is shown (black line). Note that vertical scale is kilometers.

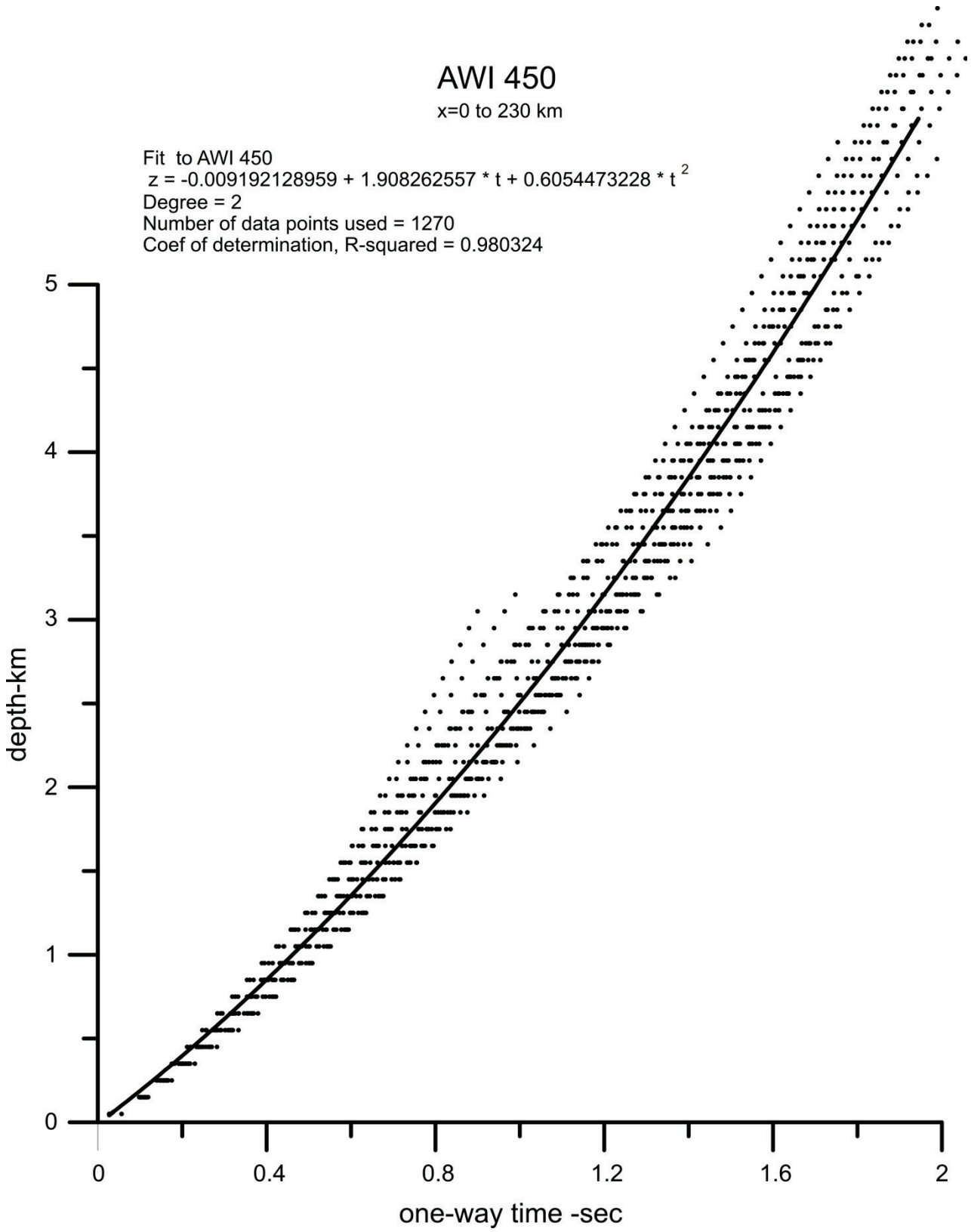

Figure A6. Depth vs time for profile AWI-20080450 seismic profile (Altenbernd et al., 2015). The polynomial fit to the data is shown (black line). Note that vertical scale is kilometers.

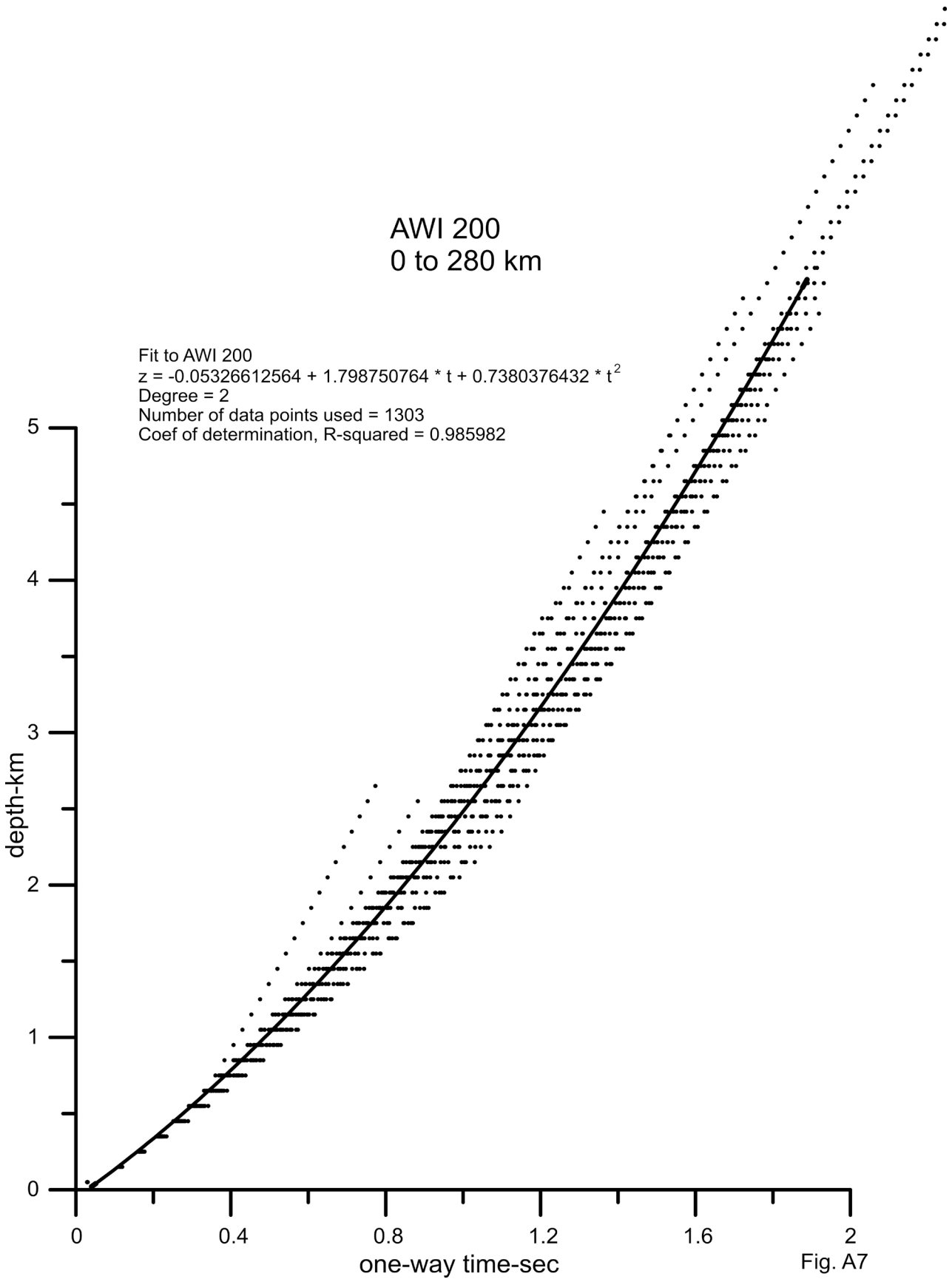

Figure A7. Depth vs time for profile AWI-20080200 seismic profile (Altenbernd et al., 2014).The polynomial fit to the data is shown (black line). Note that vertical scale is kilometers.

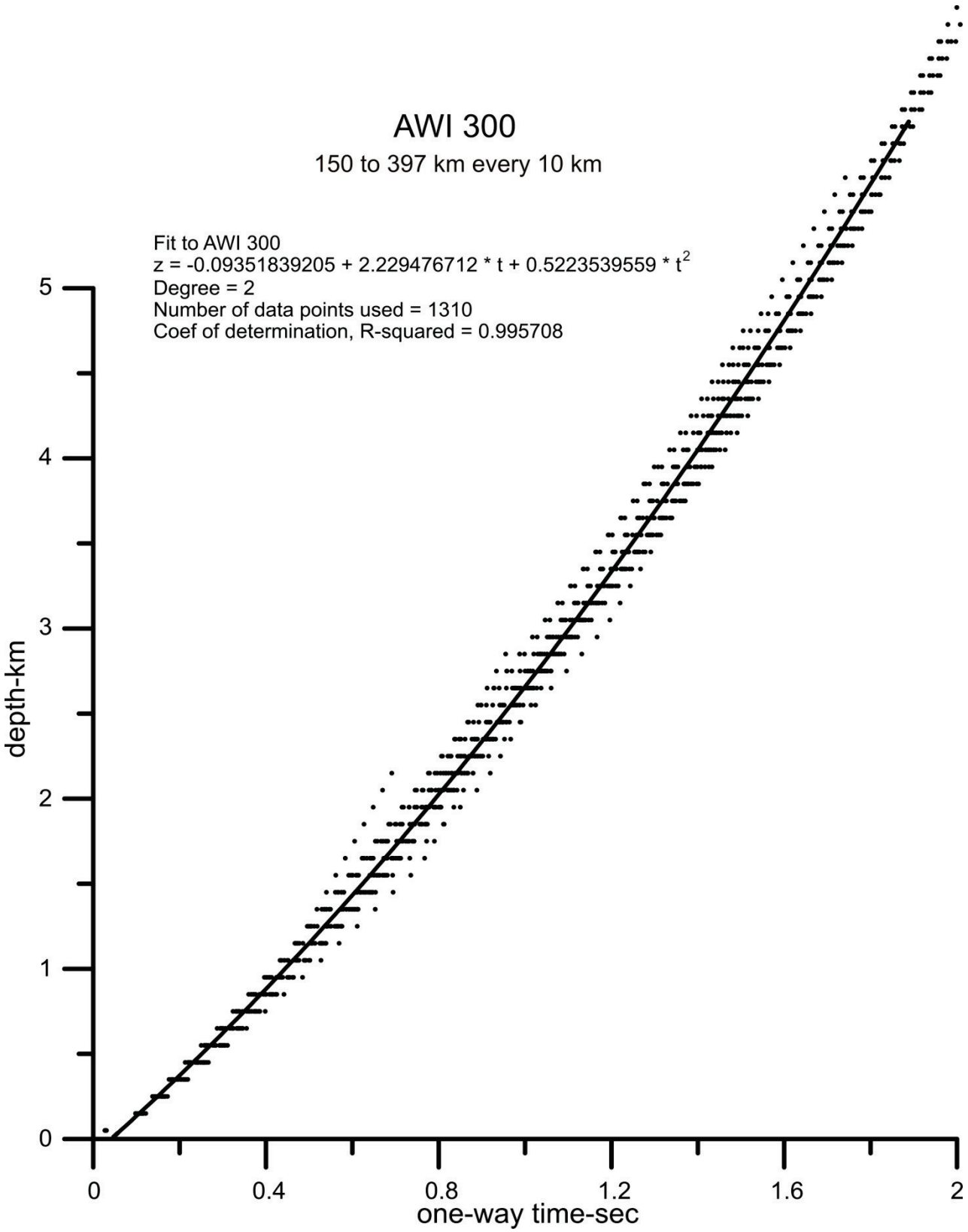

Figure A8. Depth vs time for profile AWI-20080300 seismic profile (Altenbernd et al., 2016).The polynomial fit to the data is shown (black line). Note that vertical scale is kilometers.